CIRP Journal of Manufacturing Science and Technology 41 (2023) 501–523

Contents lists available at ScienceDirect

CIRP Journal of Manufacturing Science and Technology

journal homepage: www.elsevier.com/locate/cirpj

A tribological characterisation of Ti-48Al-2Cr-2Nb and Ti-6Al-4V alloys with dry, flood, and MQL lubricants

Abhishek V. Hukkerikar [a,*,1], Pedro-J. Arrazola [a], Patxi Aristimuño [a], Susanne Norgren [b], Antoine Morandeau [c], Damien Joly [c]

[a] Mondragon Unibertsitatea, Faculty of Engineering, Loramendi 4, Arrasate - Mondragón 20500, Spain
[b] Division of Production and Materials Engineering, Lund University, Ole Römers väg 1, Lund, Sweden and Sandvik Coromant R&D, Lerkrogsv.13, 12680 Stockholm, Sweden
[c] Advanced Assisted Manufacturing Solutions, Rue Henri Garih, 37230 Fondettes, France

ARTICLE INFO

Available online 1 February 2023

Keywords:
Gamma titanium aluminides
Ti-6Al-4V
Tribology
AlTiSiN coatings
Pin-on-cylinder testing
Friction and Adhesion
Coating wear

ABSTRACT

The development of cutting tools requires the knowledge of tribological phenomena at the tool – workpiece contact area. This knowledge is in dearth particularly for *difficult-to-cut* alloys like gamma titanium aluminide (gamma – TiAl alloys). Therefore, this article is an attempt to plug the gap and aid the development of cutting tools for gamma – TiAl alloys. To this end, friction, adhesion, and coating wear between AlTiSiN coated cemented carbide tool and Ti-48Al-2Cr-2Nb (Near lamellar), Ti-48Al-2Cr-2Nb (Duplex), and the most used titanium alloy of Ti-6Al-4V (alpha – beta) were experimentally derived. A Pin-on-Cylinder (PoC) tribometer with contact conditions corresponding to commercial machining conditions was used with dry, flood(EML), and two MQL lubricants. Additionally, the heat generated and partitioned between the pin and workpiece was quantified to assess the thermal exposure to the coatings. The results showed that Ti-6Al-4V had approximately 50% higher apparent friction coefficient than the Ti-48Al-2Cr-2Nb alloys. Interestingly, the friction coefficients of Ti-48Al-2Cr-2Nb alloys were nearly consistent across the entire test matrix. Notably, the change in the microstructure from near lamellar to duplex did not elicit any qualitative or quantitative change in the friction profile of Ti-48Al-2Cr-2Nb alloys. The contact pressure proved to be the statistically significant property influencing friction evolution inversely for Ti-6Al-4V alloy and directly for Ti-48Al-2Cr-2Nb alloys. The results showed higher probability of coating wear in dry conditions as opposed to the flood and MQL lubricants.

Introduction

Global warming and climate change have compelled the United Nations (UN) to adopt strong measures to curtail carbon emissions. In this context, many industrial sectors have taken action to reduce their carbon footprints. A working paper published by [14] shows that the airline industry was responsible for 543 million tons of Carbon-dioxide (CO_2) emissions. The study outlines various steps to reduce the carbon footprint by taking several corrective measures. One of the important measures is to improve the efficiency of aircraft by using lightweight alloys in aircraft bodies and aeroengines. The gamma-TiAl alloys are a good fit for the given framework. Gamma-TiAl alloys are 50% lighter than nickel-based superalloys and have the potential to replace them in Low Pressure Turbine (LPT) section of aeroengines [12]. Additionally, their properties of high melting point, low density, high specific strength, and good structural stability [1] add to their suitability for application in aeroengines. Thus, currently, there are up to 190,000 LPT blades made of gamma-TiAl alloys in service in Boeing 787 and Boeing 747–8 aircrafts [4].

To date, three different generations of gamma-TiAl alloys have been developed. First-generation Ti -(42–48)Al alloys were found to be unsuitable for most applications owing to their low ductility and creep strength [4]. These shortcomings were addressed in second-generation alloys by the addition of Cr, Nb, Ta, Mo, and W [29], which ensured a good balance of processing, ductility, oxidation resistance, and strength [27]. An increase in the efficiency of jet engines required new formulations stable beyond the working temperature (700 °C) of second-generation gamma-TiAl alloys [5]. This necessity led to the development of third-generation alloys rich in β stabilisers such as Nb and Mo and lean in Al. However, despite these advances,

* Correspondence to: Department of Mechanical Engineering, Mondragon Unibertsitatea, Uribari 19, Arrasate-Mondragon 20500, Spain.
E-mail address: abhishek.hukkerikar@outlook.com (A.V. Hukkerikar).
[1] ORCID ID: 0000-0002-7786-2018.

https://doi.org/10.1016/j.cirpj.2022.11.016

the second-generation Ti-48Al-2Cr-2Nb alloy remains the most widely adopted, with 1,600,000 lb in active service till 2016 [4]. Of the four microstructures (*fully lamellar, duplex, near lamellar, and globular)* [17] reported for dual-phase gamma-TiAl alloys, *fully lamellar* and *duplex* microstructures are preferred because of their high fracture toughness and good ductility at room temperature [13]. A *globular* microstructure is usually avoided in material applications because of its poor ductility at room temperature [7]. Interestingly, not much has been reported regarding the applicability of *near lamellar* microstructures. A good balance between the tensile strength and ductility at room temperature makes this microstructure an interesting candidate for aeroengine applications.

Despite the obvious advantages, the use of gamma-TiAl alloys has not been extended to other aeroengine applications, such as fans, compressors, and combustors. This could be due to the high material and processing costs and poor machinability. The material properties of high hardness, low thermal conductivity, high elevated strength, and low fracture toughness [15] add to the machining difficulties. Consequently, excessive heat is generated at the tool–-workpiece interface, leading to accelerated tool wear, premature tool failure [24], and subsurface microstructural defects such as cracks, pits, and steps. The development of dedicated tool concepts can improve the machinability of these alloys. Currently, however, very little work has been published on this topic. Most tool development is undertaken with Ti-6Al-4V as the reference as it is the most widely used titanium alloy, accounting for 45–60% of the total titanium alloy production [19]. In this context, the tribological properties at the tool–workpiece interface are the central pillars in the development of new tools.

Different methodologies for tribological characterisation of tool–workpiece contact during machining and their comparison were provided by [20]. Although newer methodologies [23] have been proposed, the literature [10,20] indicates that open-configuration tribometers are more accurate in characterising the tribological properties of tool–workpiece contacts. Notably, Arrazola et al. [2] and Claudin et al. [10] reported a lack of tribological data from a machining context. Although some friction and wear evaluation studies involving gamma-TiAl alloys have been conducted, there are some shortcomings. Li et al. [18] investigated the sliding wear and friction properties of a Ti-48Al-2Cr-2Nb alloy with steel, WC, Si_3N_4, and Al_2O_3 counter materials, using a ball-on-disc tribometer. The study comprised various tool grades and derived contact parameters from Hertzian contact theory. However, only one unit of normal force measuring 10 N was used, which is not representative from a machining point of view. Additionally, the assessment was carried out only under unlubricated conditions, and a closed configuration tribometer was used. As closed configuration tribometers do not simulate the relevant tribological conditions at the tool–workpiece interface during cutting [20], the results are not the best representation of tribological phenomena at machining conditions. The studies conducted by Rastkar and Bell [25] also used a ball-on-disc tribometer. Additionally, machining tests conducted on gamma-TiAl alloys by [3,16] neglected the friction component, and the tests conducted by Settineri et al. [26] used a constant friction coefficient derived from orthogonal turning tests. Thus, it can be seen that there is a lack of tribological data for gamma-TiAl from a machining perspective. No study has been found which provides a comprehensive tribological assessment of the friction between the tool and workpiece, the role of adhesion, and the effect of thermal energy and lubricants on tool coatings. Furthermore, there are no published data explaining the role of the microstructure in the evolution of the tribological data of these alloys.

Therefore, the present study characterises the tribological properties of friction, adhesion, coating wear, and heat partitioning of Ti-48Al-2Cr-2Nb (Near lamellar) and Ti-48Al-2Cr-2Nb (Duplex) alloys. These were then compared to the results of the same tests conducted on the benchmark Ti-6Al-4V alloy. A pin-on-cylinder methodology was utilised with WC-Co pins, some uncoated and other coated with AlTiSiN. Four lubricants (Dry, Flood (emulsion mixed with water), MQLSE1, MQLVP) were utilised for the study. A central composite design was used to generate the test matrix, and the contact conditions were derived using Hertzian contact theory.

Materials and methods

Optical microscopy

The samples for optical metallography were extracted along the axis of the ingot by wire Electro Discharge Machining (EDM). Sample preparation was performed by moulding, grinding, polishing, and subsequently etching with Kroll's reagent (97 ml H_2O, 2 ml HNO_3, and 1 ml HF). The Ti-6Al-4V alloy was forged and subsequently heat-treated at 1223 K for 140 ± 5 min, followed by continuous cooling to room temperature for 105 ± 2 min. The resulting microstructure comprised of α grains surrounded by β grain boundaries, as shown in Fig. 1(a). The Ti-48Al-2Cr-2Nb bars were produced via Induction Skull Melting (ISM) and by subsequently cast via centrifugal metal die casting process. After casting, a few ingots were subjected to Hot Isostatic Pressing (HIP) and Heat Treatment (HT) to obtain duplex microstructures. The HIP was carried out at 1423.15 K in an argon atmosphere at 175 ± 10 MPa for a dwell time of 360 ± 30 min. Both the heating and cooling rates were adjusted to 10 K/min. The HT was done in the (α + γ) region at 1473 K with a dwell time of 120 ± 10 min and a cooling rate of 15 K/min. While the cast ingot exhibited a near-lamellar microstructure, as shown in Fig. 1(b), the cast + HIP + HT ingot comprised of a duplex microstructure, as shown in Fig. 1(c).

Pin-on-cylinder tests

Tribological characterisation was carried out using a Computer Numeric Control (CNC) Victor Taichung V-turn A26 machine with a traverse (X/Z) of 260/1300 mm. The Tribometer (comprising a Kistler 9129AA dynamometer and a fixture to hold the pin) was based on the design of Zemzemi et al. [30] and was mounted on a CNC lathe (Fig. 2a). A special fixture was developed to hold the MQL pipe in place, as shown in Fig. 2b. The spherical pins placed in the tribometer simulated the tool, whereas the cylindrical bars of the alloys simulated the workpiece.

The pins had an external diameter of 8 mm and spherical head radius of 6 mm. The heads were coated in two layers: (*i*) a nano-layered AlTiN inner part coating with modulation of the aluminium content over the total layer thickness, and (*ii*) a nano-layered outer coating of AlSiTiN. The average coating thickness on the external surface was 2–5 µm. To eliminate any inconsistencies during the experiments, the pins were polished to achieve a surface roughness of < 0.8 µm. After each test, a cutting tool was used to remove the surface ploughed by the pin. This ensured that pin traced a refreshed surface for every experiment.

The contact conditions were chosen keeping in mind the commercial machining conditions. Based on the state of the art [22], the P_{avg} from 1.31 to 3.27 GPa and v_s between 35 and 125 m/min were chosen for this study. The experimental plan is explained in detail in *Design of experiments*. The μ_{app} is equivalent to the ratio of the tangential to normal forces, as presented in Eq. (1). The friction coefficient is termed as the "*Apparent friction coefficient*, as it varies significantly from the "*Local friction coefficient*" for a given instance. The μ_{app} can be further decomposed into adhesive and plastic deformation components. The contribution of each component to the μ_{app} was estimated in accordance with calculations reported by Claudin et al. [11].

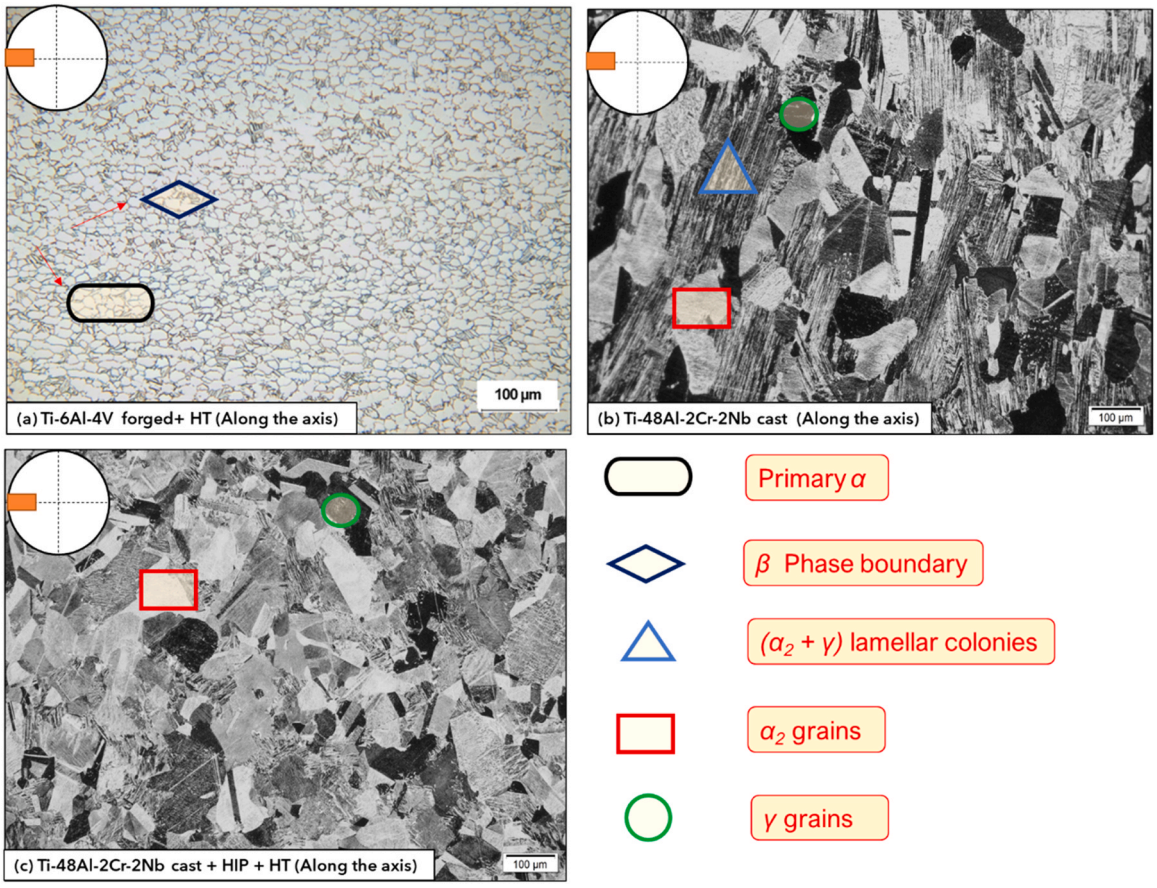

Fig. 1. The optical micrographs of (a) Ti-6Al-4V (forged + HT), (b) Ti-48Al-2Cr-2Nb (Cast), and (c) Ti-48Al-2Cr-2Nb (Cast + HIP + HT).

$$\mu_{app} = \frac{F_t}{F_n} = \mu_{adh} + \mu_{plast} \tag{1}$$

where μ_{app} is the apparent friction coefficient, F_t and F_n are the tangential and normal forces and, μ_{adh} is the adhesive friction component and μ_{plast} is the plastic friction component.

The required F_n for a given P_{avg} were determined using Hertzian conditions. The Hertzian contact conditions accommodate Poisson's ratios and Young's moduli of the alloys while calculating the F_n. While the Poisson's ratios of all the alloys were adopted from the literature [8], the corresponding Young's moduli were calculated through ultrasound analysis as shown in Eq. (2):

$$E = \frac{\rho v_t^2 (3v_l^2 - 4v_t^2)}{(v_l^2 - 2v_t^2)} \tag{2}$$

The ultrasonic probe producing sonic waves was incident along and across the bar axes during the analysis. The probe captured the longitudinal (v_l) and transversal (v_t) propagating velocities, which when computed along with density ρ as shown in Eq. (2), yielded the Young' modulus E. The material properties of the pins were provided by AB Sandvik Coromant. The results are presented in Table 1 as follows:

The next step involves the assessment of the contact radius (a) of the pin, incident on the workpiece as shown in Eq. (3):

$$a = \sqrt[3]{\frac{3*F_n}{8} * \left[\frac{\frac{1-\nu_1^2}{E_1} + \frac{1-\nu_2^2}{E_2}}{\frac{1}{2*R_1} + \frac{1}{2*R_2}} \right]} \tag{3}$$

where v_1 *and* v_2 are Poisson's ratios, E_1 and E_2 are the elastic moduli, and R_1 and R_2 are the radii of the pin and workpiece surface, respectively. While R_1 had an established radius, R_2 was considered infinite for long cylinders in accordance with Hertzian contact conditions. Finally, the required F_n for a given contact pressure P_{avg} and known contact radius a was obtained from Eq. (4):

$$F_n = \frac{P_{avg} * 2 * \pi * a^2}{3} \tag{4}$$

The F_n and F_t were continuously recorded during the experiments. The mean values of forces in the stable region, as shown in Fig. 3, were used to compute the corresponding μ_{app} value.

Four lubricants, dry, flood (EML), MQLSE1, and MQLVP, with physiochemical properties listed in Table 2, were used in this study. The EML with a concentration of 10–11% was delivered via the turret at a flow rate of 25 *l*/min and pressure of 15 bar. The MQL oils were delivered via a tube fixed at 30º to the workpiece, as shown in Fig. 2(b). A special fixture was used to ensure that the tube remained in position during the experiments. The optimum distance between the tube outlet and spherical surface of the pins was determined to be 8.2 mm before the trials. The flow rate of both MQL oils was set at 70 ml/h with a pressure of 2.5 bar.

Special care was taken to ensure that the *K*-type thermocouple wires did not become entangled with each other or any moving elements to prevent inaccuracies during temperature measurements. Holes of ∅ = 1 mm with axis perpendicular to the axis of the pin were cut with EDM to house thermocouple wires for temperature measurements. The dimension of the pin and thermocouple holes are presented in Fig. 4.

The adhesion of the workpiece to the pins and coating wear was studied using a Keyence Numerical Microscope VHX 5000 series with a tolerance of 50 µm in both the X- and Z-coordinate axes. The

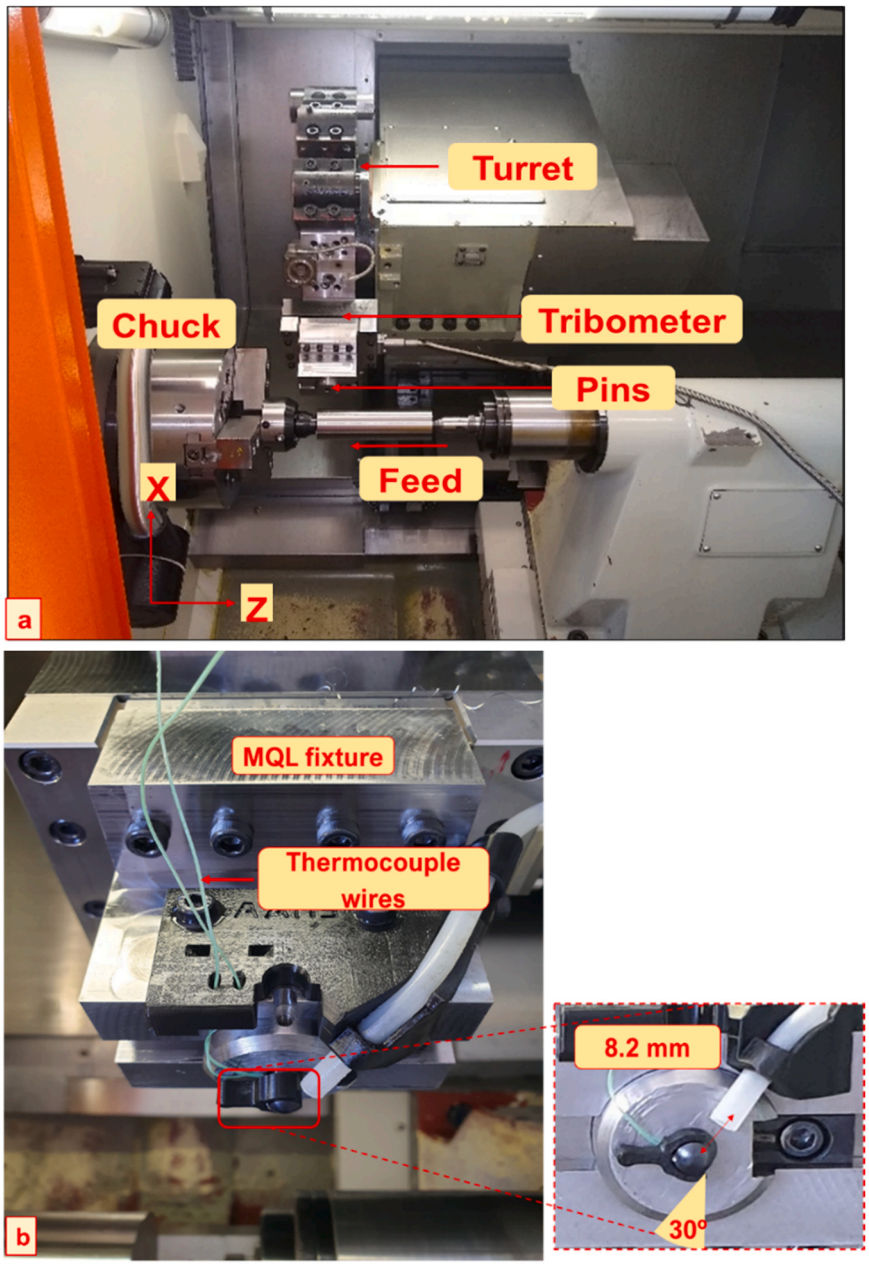

Fig. 2. The experimental setup showing (a) Pin-on-Cylinder Tribometer for dry and flood conditions (b) Special fixture for MQL lubricants.

wear debris on the pin surface was analysed using an 18 megapixel mera with a 3CMOS 50 fps.

Any *accumulated particles* comprising dust, loose workpiece debris, microchips, etc. (Fig. 5a) were then removed using a single swipe of clean paper. This revealed the sticking area, which was then digitally quantified (Fig. 5b). Any wear on the coating was observed beneath the *sticking area*.

Therefore, a few selected pins (with lowest and highest P_{avg} of 1.31 and 3.27 GPa and constant v_s = 80 m/min) were chosen for cross section analysis. The cross section analysis was conducted after the friction assessment, wherein it was found that P_{avg} was the statistically significant property. This has been explained in detail in *Results and discussion*. Thus, pins with different P_{avg} but with same v_s were chosen for the analysis. The Fig. 6(a–b) show the *sticking area*

Table 1
Material properties obtained from ultrasound analysis and the literature.

Material	Material properties		Source / Reference
	Poisson's ratio ν	Youngs Modulus, E, (GPa)	
Ti-6Al-4V	0.34	100 ± 8	ν: [7]; E: Empirically derived
Ti-48Al-2Cr-2Nb (NL)	0.23	158 ± 11	ν: [7]; E: Empirically derived
Ti-48Al-2Cr-2Nb (D)	0.23	155 ± 14	ν: [7]; E: Empirically derived
Pin	0.225	600	AB Sandvik Coromant

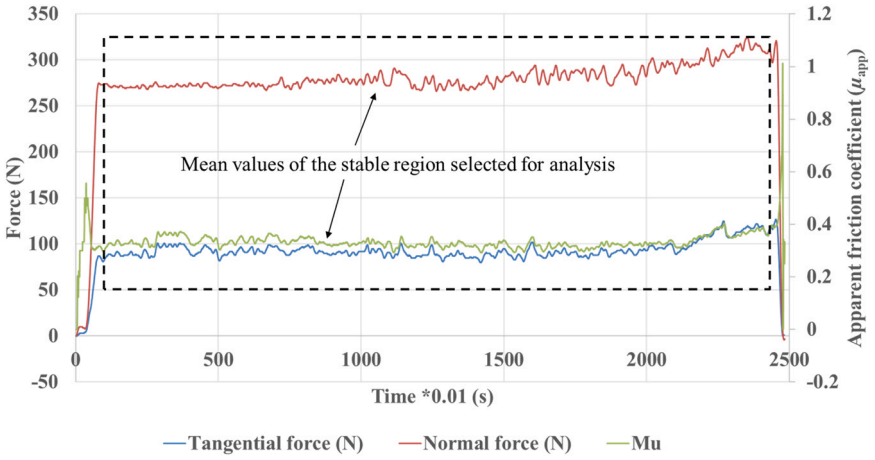

Fig. 3. Variation of normal and tangential forces during the experiment and the corresponding apparent friction coefficient.

Table 2
Physical-Chemical data of all lubricants.

Physical – Chemical data	Concentrate EML	EML (Mixed with water) Vasco 7000	MQL SE 1	MQLVP
Density at 15ºC, kg/m^3		Close to water	0.876	0.907
Density at 20ºC, kg/m^3	0.98	Close to water	0.873	0.904
Viscosity at 40ºC, mm^2/s	74 mm^2/s	Close to water	19.8	23.1
Flash point, ºC	134	–	176	255
Specific heat (J/ kg. K) (Literature values)		Close to water	1.97	1.97
pH value		8.8 – 9.5	NA	NA
Nature	Ester based		Ester based oil with additives	Ester based oil with additives

and its quantification. The Fig. 6(c) shows the procedure adopted to cut, grind, polish and mould the pins, while the Fig. 6(d) presents the optical micrograph showing the coating wear assessment.

The total power consumed during the tests is expended as plastic deformation of the softer material and friction between the workpiece and pin. The breakdown is represented by Eq. (5), as follows:

$$P_g = P_{pd} + P_f = F_t{}^* v_s \tag{5}$$

A pictorial representation of heat distribution between pin and workpiece is shown in Fig. 7. Bonnet et al. [6] state that 90% of the power during plastic deformation is converted to heat, 10% is devoted to strain hardening The heat consumed during strain hardening is dependent on properties such as the density, specific heat, temperature gradients, tensor stress, and strain rate of the material during the process, requiring dedicated measurements.

As the quantification of heat due to strain hardening is difficult, this component of plastic deformation was omitted in the present study. Assuming that the entire power consumed by the frictional component is converted to heat, the remaining friction power can be calculated as represented in Eq. (6), as follows:

$$P_f = F_{tlocal}{}^* V_{slocal} = \varphi_{friction} \tag{6}$$

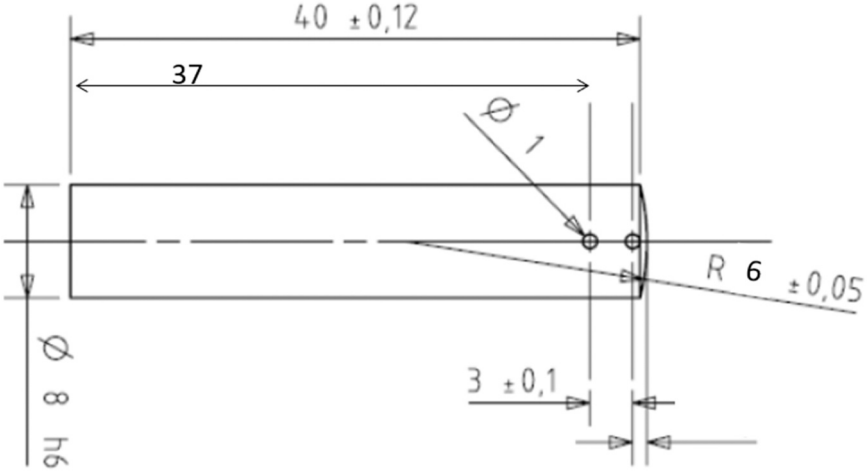

Fig. 4. The EDM holes on the pins for the placement of thermocouple wires during temperature measuring experiments.

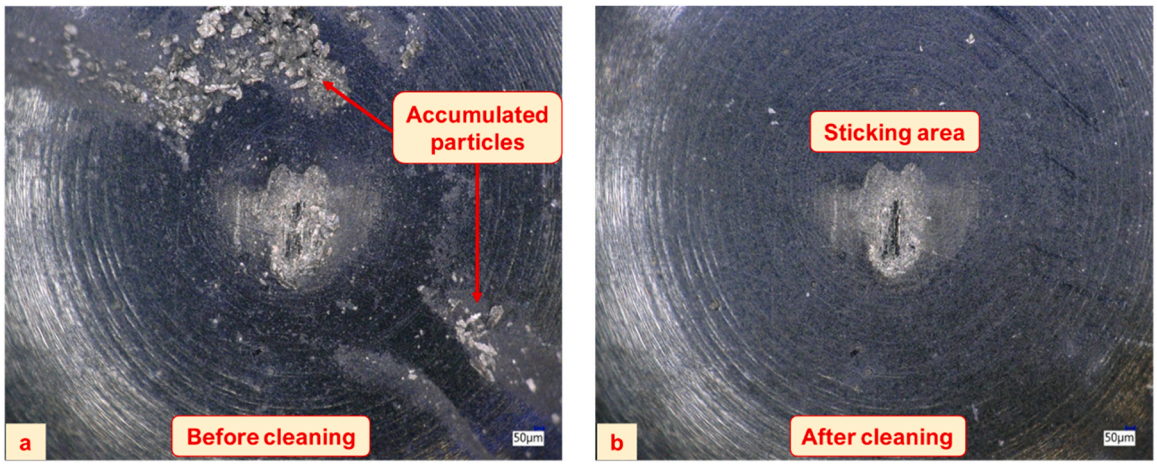

Fig. 5. The procedure to clean the pins and the appearance of pins (a) before cleaning (b) after cleaning.

The heat dissipated during the friction tests can be subdivided into frictional heat entering the workpiece and frictional heat entering the pin, as shown in Eq. (7):

$$\varphi_{friction} = \varphi_{friction-WM} + \varphi_{friction-pin} \tag{7}$$

The instantaneous heat flow entering the pins was measured by measuring the temperature difference between the thermocouples. The thermocouples were placed as shown in Fig. 3. The temperature difference was translated to heat in accordance with the Eq. (8) given by [22] as:

$$\varphi_{friction-pin} = \lambda^* S_{pin} * \frac{\Delta T}{dx} \tag{8}$$

where the $\varphi_{friction\ -\ pin}$ is the flux entering the pin, λ is the thermal conductivity of the pin, S_{pin} is the pin cross-sectional area, ΔT is the temperature difference measured in the pin, and dx is the distance between thermocouples. The heat transmitted to the pins (β) is calculated as shown in Eq. (9):

$$\%\beta_{pin} = \frac{\varphi_{friction-pin}}{\varphi_{friction}} \times 100 \tag{9}$$

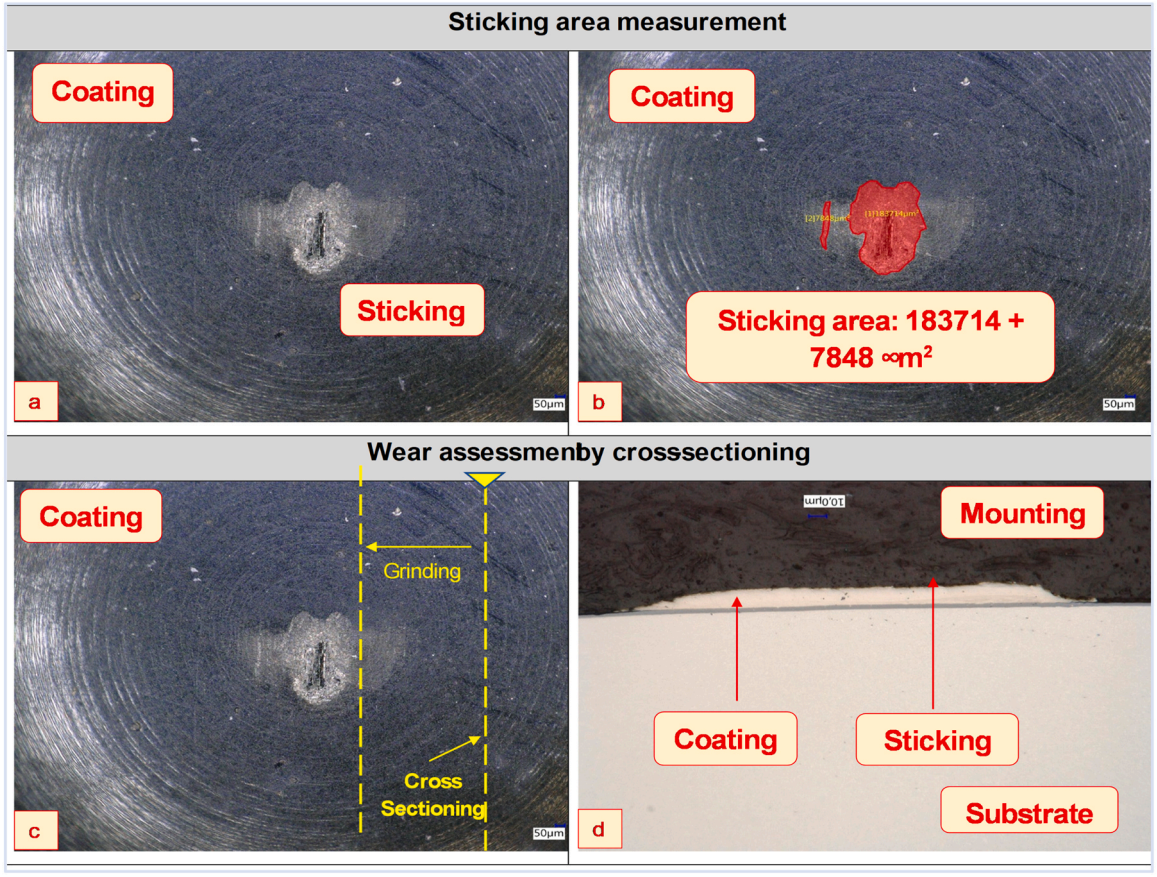

Fig. 6. Cross-sectioning procedure for selected pins showing the appearance of (a) sticking area (b) the quantification of sticking area (c) the procedure to slice the pins and (d) assessment of coating wear.

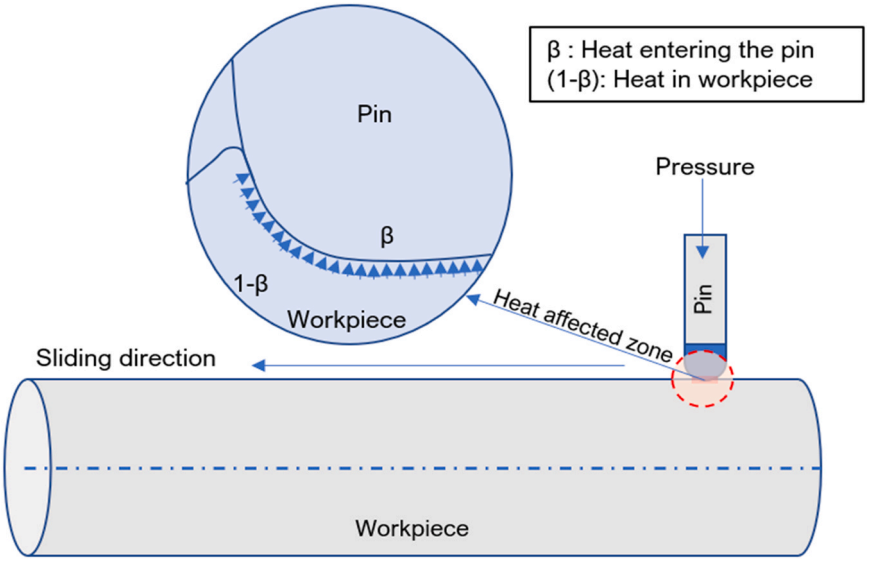

Fig. 7. Pictorial representation of quantification of heat between pin and workpiece during POC tests.

where % β_{pin} is the percentage of heat entering the pins, and the rest entering the workpiece.

Design of experiments

The P_{avg}, and v_s of the pin were the input parameters of the study. The F_n for a given P_{avg} was derived as shown in *Pin-on-Cylinder tests*. The μ_{app} was the output parameter. The experimental plan had to accommodate many considerations. To begin with, all the contact conditions that exist during machining had to be experimented i.e., the range of P_{avg} from (1–3 GPa) combined with range of v_s (35–120 m/min). These conditions have been reported by [22]. Next, the combination of each contact condition had to be experimented with each of the three lubricant types (Dry, Flood (EML), and MQL). For example, 1.31 GPa + 37.50 m/min with each of dry, MQL, EML lubricants. In addition, this was to be carried out for each of the three alloys. Therefore, optimisation of resources (pin substrates and coating) was paramount.

Thus, to include all the foregoing aspects, a Central Composite Design (CCD) as described by [9] was used to develop the test matrix. For each alloy and a lubricant combination (For ex. Ti-48Al-2Cr-2Nb (NL) with EML), 11 experiments inclusive of three repetitions at the central points (2.30 GPa and 80 m/min) were designed. The differences arising from the repetitions were termed as the uncertainty. The uncertainty was applicable to each experiment in the test matrix in accordance with the CCD methodology. The test matrix is set out in Table 3.

Additionally, experiments were performed randomly without any set order to avoid any potential errors arising due to incremental order of P_{avg}. For example, if the first experiment was done with 2.30 GPa + 80 m/min, the next was done with 1.60 GPa + 110 m/min, and the next with 2.30 + 37.5 m/min and so on. A total of 132 tests were conducted with all lubricants.

A few tests with uncoated substrates were also carried out to know the effectivity of coatings. However, these were performed only at the central points of 2.30 GPa + 80 m/min. This was done due to the limited stock of the pins. The results of uncoated pins were later compared with the corresponding central points of coated pins to assess the coating efficiency. A total of 36 uncoated tests were conducted comprising of all lubricants. The total number of tests carried out are shown in Table 4 as follows:

The μ_{app} values obtained by the experiments were subjected to response surface modelling to assess the evolution of the μ_{app} as a function of P_{avg}, and v_s.

Results and discussion

The results of friction, adhesion, and heat partition analysis have been tabulated in Tables 5–7 respectively. A discussion of this results is provided subsequently.

Friction profile of Ti-6Al-4V

The μ_{app} for Ti-6Al-4 V was almost 50% higher than the Ti-48Al-2Cr-2 Nb (near lamellar and duplex) alloys. The results showed that the μ_{app} values were the highest in dry conditions, followed by EML and MQLSE1, as presented in Table 5. MQLVP exhibited comparatively lower μ_{app} values. For all lubricants, an increase in the P_{avg} led to a decrease in μ_{app}, indicating an inversely proportional relationship between P_{avg} and μ_{app}. Thus, the P_{avg} was statistically significant property. On the other hand, the v_s showed conflicting trends depending on P_{avg} and the lubricant. Under dry conditions for P_{avg} ≤ 2.3 GPa, any increase in v_s led to a decrease in μ_{app} values. Interestingly, as P_{avg} exceeded the 2.3 GPa threshold, an increase in v_s led to an increase in the μ_{app} values. Thus, a parabolic trend for v_s was clearly observed under dry conditions. The Fig. 8 presents the friction and adhesion profile of Ti-6Al-4 V alloy with all the lubricants.

Importantly, with EML and MQLSE1, v_s presented a different profile. At a low P_{avg} (1.31 GPa), an increase in v_s led to only a marginal increase in μ_{app}, whereas at a high P_{avg}, any increase in v_s led to a decrease in μ_{app}. As seen with dry conditions, the P_{avg} proved to be the threshold value. For P_{avg} ≥ 2.3 GPa, an increase in v_s resulted in a decrease in μ_{app}. The MQLVP also confirms the observations except for one condition (1.61 GPa and 110 m/min).

Notably, the lubricants (EML, MQLSE1, and MQLVP) produced lower μ_{app} values than dry condition. This was particularly discernible at the threshold value of P_{avg} ≥ 2.3 GPa. One possible explanation is that the lubricants had a wetting effect on the asperities, making them more susceptible to fracture, thus resulting in low μ_{app} values. This is consistent with the findings of Suh et al. [28]. It appears that when P_{avg} was lower, the pins needed to overcome the higher resistance to satisfy the shearing of the asperity junctions, thereby leading to a higher μ_{app}. This outcome also proves that the

Table 3
The Central Composite Design and the test matrix for coated and uncoated pins for Ti-48Al-2Cr-2Nb (NL and D) and Ti-6Al-4V alloys.

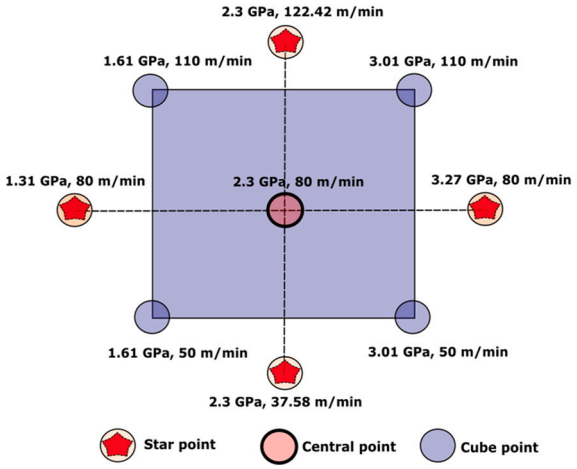

Central Composite Design for coated pins					
Test number and point	Ti-48Al-2Cr-2Nb (NL & D)		Ti-6Al-4V		Sliding velocity, v_s, m/min
	Hertzian contact pressure, P_{avg} GPa	Normal Force, F_n,N	Hertzian contact pressure, P_{avg}, GPa	Normal Force, F_n, N	
1	1.31	10	1.31	21	80
2	1.61	17	1.61	39	50
3	1.61	17	1.61	39	110
4	2.30	49	2.30	115	37.58
5	2.30	49	2.30	115	80
6	2.30	49	2.30	115	80
7	2.30	49	2.30	115	80
8	2.30	49	2.30	115	122.42
9	3.01	110	3.01	260	50
10	3.01	110	3.01	260	110
11	3.27	140	3.27	325	80
Design for uncoated pins					
13	2.30	49	2.30	115	80
14	2.30	49	2.30	115	80
15	2.30	49	2.30	115	80

lubricants were able to enter the pin–workpiece interface even at high $P_{avg} \geq 2.3$ GPa.

Adhesion profile of Ti-6Al-4V

In dry conditions, a clear trend was observed in which the adhesion area increased with an increase in P_{avg}. However, outliers were also observed; the experimental uncertainty was high (0.22). While two repetitions yielded almost similar values of 0.63 mm^2 and 0.66 mm^2, the third repetition yielded a lower value of 0.23 mm^2. At P_{avg} = 2.3 GPa + v_s = 122.42 m/min, an adhesion area of 1.10 mm^2 was recorded. This value was unusually high considering that all the other experiments yielded values of < 0.67 mm^2. Thus, this value is more likely to be an aberration. If this value is considered as an outlier, then the dry lubricant trend indicates that increased P_{avg} led to a higher amount of sticking material or higher adhesion (Fig. 8a). It also seemed that less material was able to exit the bodies in contact at a high P_{avg}, thereby increasing the amount of entrapped material. However, this observation needs validation by the measurement of the adhesion volume.

As presented in Fig. 8, the adhesion profiles of all the lubricants were found to be in the same range, indicating that all were equally effective in retaining similar amounts of workpiece material at the pin–workpiece interface. A comparison of the adhesion profiles of pins with all lubricants is presented in Table 8. The low adhesion area of the lubricants in comparison to dry conditions suggests that the lubricants were able to enter the pin–workpiece interface and wash away most of the wear debris. Claudin et al. [11] corroborated that lubricants can enter the interface, even at a high P_{avg} of > 2 GPa. This trend was visible even up to 3.01 GPa with a low v_s = 50 m/min, in which the average adhesion area was 0.21 mm^2. However, for the same P_{avg}, as v_s increased to 110 m/min, the adhesion area surged to 0.49 mm^2. This shows that v_s plays an important role in the increase or decrease of the adhesion area up to a P_{avg} value as high as 3.01 GPa.

Experiments with EML also revealed the critical role played by v_s, but only at high P_{avg} values (Fig. 8b). When v_s increased from 50 m/min to 110 m/min at a low P_{avg} of 1.61 GPa, no substantial increase in the adhesion area was recorded. Thus, at a lower P_{avg}, the lubricant could enter the interface easily, and any modulation of v_s did not hinder it from providing the wetting effect of the asperities, aiding shear. However, at a high P_{avg} of 3.01 GPa, a change in v_s from 50 to 110 m/min led to a surge in the adhesion area, as observed previously under dry conditions. This observation is also in agreement with the findings of [11], who found that the duration of the lubricant at the pin–workpiece interface is dependent on v_s. Thus, it appears that increasing v_s allows less time for the lubricant to wash away the wear debris, thereby increasing the adhesion area.

In the case of MQLSE1 (Fig. 8c), the pure error/uncertainty arising from repetitions was high. While two repetitions yielded 0.17 mm^2 and 0.12 mm^2, the third experiment yielded 0.33 mm^2. The trends were quite similar to those of the EML, where the adhesion area increased with an increase in P_{avg}. The dependency of v_s was also similar to that observed in the EML. Additionally, the μ_{app} appeared to be independent of the adhesion area and coating at 2.30 GPa + 80 m/min.

Importantly, it could be recalled that MQLVP exhibited a lower μ_{app} than the other lubricants. Although its adhesion area increased with the increase in P_{avg} (Fig. 8d), the increase was not as drastic as that observed with other lubricants. For example, at a high P_{avg} of 3.01 GPa, the adhesion area remained at 0.28 mm^2 even after v_s increased from 50 to 110 m/min. This shows that MQLVP was able to achieve better lubrication at the interface. As seen in the previous lubricants, μ_{app} appeared to be independent of the adhesion area and coating at 2.30 GPa + 80 m/min.

A comparison of friction profiles between the uncoated and coated pins at the threshold conditions of 2.30 GPa + 80 m/min yielded interesting outcomes. The uncoated pins were more effective in reducing friction than the coated pins under dry conditions. With lubricants, the uncoated pins performed similarly as coated pins. In order to validate the better performance of uncoated pins in dry condition, a track analysis was conducted. The objective of the analysis was to verify the surface quality of the workpiece against the uncoated pins. Interestingly, the surface of the material was smooth and crack-free, as shown in Fig. 9.

A significant difference in adhesion area was observed between the uncoated and coated pins. Although the μ_{app} of the uncoated pins was lower than (dry conditions) or equal to (EML and both MQL oils) that of the coated pins, the adhesion area was found to be greater. Remarkably, the adhesion did not alter the μ_{app}. Thus, it appeared that μ_{app} was independent of the adhesion area at 2.30 GPa + 80 m/min. Clearly, Ti-6Al-4 V was found to be better suited for uncoated pins as they were effective in reducing friction than coated pins, at the threshold conditions. However, further experiments are

Table 4
Experimental programme of POC tests in lubricated and unlubricated conditions.

Experimental plan for Pin on Cylinder tests with all lubricants						
Coated				Uncoated		
Phase	Material	Lubricants	DoE	Material	Lubricants	Normal
Phase1: Dry	NL	None	11	NL	None	3
	D	None	11	D	None	3
	Ti64	None	11	Ti64	None	3
Phase 2: Lubricants	NL	EML	11	NL	EML	3
	D	EML	11	D	EML	3
	Ti64	EML	11	Ti64	EML	3
	NL	MQLSE1	11	NL	MQLSE1	3
	D	MQLSE1	11	D	MQLSE1	3
	Ti64	MQLSE1	11	Ti64	MQLSE1	3
	NL	MQLVP	11	NL	MQLVP	3
	D	MQLVP	11	D	MQLVP	3
	Ti64	MQLVP	11	Ti64	MQLVP	3
Total tests			**132**			**36**
				NL: Ti-48Al-2Cr-2Nb (NL)		
				D: Ti-48Al-2Cr-2Nb (D)		
				Ti64: Ti-6Al-4V		

necessary to confirm this result under other contact conditions of the test matrix.

The coating wear analysis was conducted with dry, EML, and MQLSE1 lubricants. The wear analysis with MQLVP oil could not be conducted due to budgetary constraints. As P_{avg} was the statistically significant property, the pins with low (1.31 GPa) or high (3.27 GPa) P_{avg} combined with a constant v_s of 80 m/min were selected.

In dry conditions, at 1.31 GPa, the coating was uniform and continuous as seen in Fig. 10a. However, small pockets of coating erosion were detected at 3.27 GPa, as shown in Fig. 10b. Overall, the coatings were intact in both P_{avg}. However, SEM analysis is necessary to confirm these results.

With EML, at 1.31 GPa, as depicted in Fig. 11a, the coating was found to be intact. However, erosion of the coating in the form of cavities and craters was observed at 3.27 P_{avg}, as seen in Fig. 11b.

Interestingly, in the case of MQLSE1, the coating remained intact under both contact conditions. While at 1.31 GPa (Fig. 12a), the coating was nearly unaffected, at 3.27 GPa (Fig. 12b), some fissures in the coating were detected. However, these fissures did not affect the overall integrity of the coatings.

The heat partition assessment under dry conditions indicated that 70.1% of the total heat generated was transmitted to the pins. As expected, the heat generated was the highest under dry conditions (51.5 W). Owing to the high cooling properties of the EML, less heat was generated and transmitted to the pins. The heat incident on the pins was only 32.69 W. The MQLSE1 also performed similar to EML, and subsequently let only 37.14 W of heat to the pins. Though this heat is slightly high in magnitude, it highlights that the lubricating properties of MQL are equally efficient to the cooling properties of EML for the given contact conditions. The MQLVP performed better than the dry conditions but was 5% less efficient than MQLSE1.

Milton et al. [21] report that the adhesion on the pins is an important aspect which determines the heat partition between the pin and workpiece. Although the adhered material is mainly the workpiece material, the added dust and foreign debris contaminates the workpiece material, preventing heat from reaching the pins. Therefore, a possible explanation of coating remaining intact in dry

Table 5
Apparent friction coefficients of Ti-6Al-4V and Ti-48Al-2Cr-2Nb (NL and D) with dry, EML, MQLSE1 and MQLVP lubricants.

Contact pressure, (GPa)	Sliding Velocity, (m/min)	App. Friction coefficient (μ_{app}) of Ti-48Al-2Cr-2Nb (NL)				App. Friction coefficient (μ_{app}) of Ti-48Al-2Cr-2Nb (D)				App. Friction coefficient (μ_{app}) of Ti-6Al-4V			
		Dry	EML	MQLSE1	MQLVP	Dry	EML	MQLSE1	MQLVP	Dry	EML	MQLSE1	MQLVP
1.31	80	0.2	0.26	0.16	0.24	0.24	0.27	0.26	0.21	0.38	0.42	0.4	0.37
1.61	50	0.29	0.28	0.24	0.26	0.24	0.28	0.25	0.27	0.45	0.35	0.4	0.31
1.61	110	0.24	0.24	0.21	0.23	0.19	0.25	0.23	0.22	0.41	0.37	0.4	0.36
2.3	37.58	0.32	0.27	0.26	0.27	0.27	0.27	0.27	0.26	0.47	0.34	0.35	0.29
2.3	80	0.23	0.24	0.24	0.22	0.23	0.25	0.24	0.26	0.46	0.31	0.29	0.3
2.3	80	0.23	0.25	0.25	0.21	0.21	0.25	0.25	0.24	0.42	0.31	0.27	0.27
2.3	80	0.24	0.24	0.24	0.21	0.23	0.24	0.23	0.25	0.46	0.3	0.27	0.28
2.3	122.42	0.23	0.23	0.22	0.25	0.26	0.22	0.23	0.26	0.4	0.32	0.3	0.26
3.01	50	0.28	0.26	0.27	0.23	0.28	0.26	0.27	0.27	0.24	0.27	0.28	0.27
3.01	110	0.31	0.29	0.32	0.26	0.31	0.27	0.3	0.3	0.3	0.26	0.23	0.22
3.27	80	0.29	0.27	0.26	0.22	0.31	0.27	0.3	0.3	0.29	0.24	0.25	0.23
Uncoated pins													
2.3	80	0.24	0.25	0.26	0.23	0.24	0.25	0.25	0.25	0.27	0.31	0.29	0.29
2.3	80	0.24	0.25	0.25	0.23	0.23	0.25	0.26	0.25	0.27	0.3	0.28	0.27
2.3	80	0.25	0.25	0.26	0.23	0.24	0.25	0.26	0.25	0.27	0.31	0.27	0.27

Scale	0.16 - 0.23	0.23 - 0.31	0.31 -

Table 6
Quantification of adhesion area of Ti-48Al-2Cr-2Nb (NL) and Ti-48Al-2Cr-2Nb (D) with dry, EML, MQLSE1, and MQLVP lubricants.

Contact pressure, (GPa)	Sliding Velocity, (m/min)	Adhesion area (mm2) of Ti-48Al-2Cr-2Nb (NL)				Adhesion area (mm2) of Ti-48Al-2Cr-2Nb (D)				Adhesion area (mm2) of Ti-6Al-4V			
		Dry	EML	MQLSE1	MQLVP	Dry	EML	MQLSE1	MQLVP	Dry	EML	MQLSE1	MQLVP
1.31	80	0.05	0.05	0.02	0.05	0.06	0.04	0.02	0.02	0.29	0.06	0.10	0.09
1.61	50	0.04	0.04	0.01	0.01	0.09	0.03	0.01	0.01	0.14	0.06	0.19	0.07
1.61	110	0.00	0.03	0.02	0.06	0.15	0.04	0.02	0.06	0.18	0.07	0.21	0.12
2.3	37.58	0.02	0.07	0.03	0.02	0.06	0.03	0.03	0.04	0.17	0.10	0.12	0.11
2.3	80	0.03	0.02	0.03	0.13	0.08	0.04	0.02	0.03	0.63	0.26	0.17	0.19
2.3	80	0.02	0.03	0.03	0.08	0.06	0.06	0.02	0.06	0.23	0.19	0.12	0.17
2.3	80	0.02	0.03	0.05	0.08	0.09	0.08	0.03	0.07	0.66	0.20	0.33	0.19
2.3	122.42	0.05	0.05	0.06	0.10	0.11	0.06	0.02	0.05	1.10	0.26	0.25	0.24
3.01	50	0.06	0.07	0.08	0.08	0.1	0.10	0.06	0.05	0.23	0.21	0.24	0.28
3.01	110	0.16	0.15	0.08	0.14	0.21	0.15	0.11	0.08	0.67	0.49	0.39	0.28
3.27	80	0.13	0.11	0.07	0.10	0.15	0.13	0.12	0.08	0.62	0.51	0.52	0.34
Uncoated pins													
2.3	80	0.045	0.07	0.06	0.06	0.04	0.13	0.06	0.06	0.31	0.31	0.26	0.23
2.3	80	0.052	0.06	0.05	0.08	0.04	0.07	0.05	0.06	0.33	0.30	0.22	0.22
2.3	80	0.056	0.07	0.06	0.06	0.06	0.07	0.06	0.06	0.27	0.33	0.21	0.22

Scale: 0.01 - 0.06 | 0.07 - 0.34 | 0.34 -

Table 7
The Heat partition coefficients of all alloys under all lubrications calculated at 2.3 GPa and 80 m/min.

Alloys / Thermal properties	Ti-48Al-2Cr-2Nb (NL)				Ti-48Al-2Cr-2Nb (D)				Ti-6Al-4V			
	Dry	EML	MQL SE1	MQLVP	Dry	EML	MQL SE1	MQLVP	Dry	EML	MQL SE1	MQLVP
Temperature difference recorded by the thermocouple, ΔT, (K)	8.9	1.8	4.5	3.5	8.2	2.66	4.56	6.33	24.33	11	12	13.33
Tangential force, F_t, (N)	12.23	12.19	12.72	10.64	11.28	12.19	11.65	12.33	38.72	37.56	36.04	35.42
Sliding velocity, v_s, (m/s)	1.33											
Total heat generated during tests, $\varphi_{friction}$, (W)	16.27	16.21	16.91	14.15	15	16.21	15.5	20.47	51.5	49.95	47.93	47.11
Heat transmitted to pins, $\varphi_{friction\text{-}pin}$, (W)	13.2	2.67	6.68	5.2	12.16	3.86	6.76	9.39	36.1	16.33	17.8	19.77
Percentage of total heat transmitted to the pin, % β_{pin}	81.13	16.47	39.5	36.74	81.06	23.81	43.61	45.87	70.1	32.69	37.14	41.96
Apparent friction coefficient, μ_{app}	0.23	0.25	0.25	0.21	0.21	0.25	0.25	0.24	0.42	0.31	0.27	0.27
Adhesion area, (mm^2)	0.02	0.03	0.03	0.08	0.06	0.06	0.02	0.06	0.23	0.19	0.12	0.17

Scale: Low | Medium | High

conditions despite generating more heat than lubricants, could be attributed to higher adhesion area of Ti-6Al-4 V alloy.

Friction profiles of Ti-48Al-2Cr-2Nb (near lamellar and duplex)

The assessment of both the alloys is presented together as both the alloys traced the same μ_{app} profiles. The μ_{app} evolution pattern of the Ti-48Al-2Cr-2 Nb (NL and Duplex) alloys was fundamentally different than the benchmark Ti-6Al-4 V alloy. As seen in Figs. 13 and 14, no large deviation of μ_{app} was seen across the entire test matrix for both the alloys with all the lubricants. The overall range of μ_{app} for both the alloys fell between 0.2 and 0.3, except in the case of Ti-48Al-2Cr-2 Nb (NL) with MQLSE1 at 1.31 GPa (μ_{app} = 0.16).

With dry and MQLSE1, μ_{app} increased with increase in P_{avg}. The MQLVP yielded different outcomes. On one hand, the μ_{app} values stayed constant across the test matrix for Ti-48Al-2Cr-2 Nb (NL) alloy. On the other, the μ_{app} increased with increase in P_{avg} for Ti-48Al-2Cr-2 Nb (D) alloy. Importantly for both the alloys, the μ_{app} values with EML were consistent and unaffected by the change in P_{avg}.

The v_s implied the existence of the threshold conditions as seen in Ti-6Al-4 V. The increase in v_s caused a decrease in μ_{app} until P_{avg} was ≤ 2.3 GPa. At this threshold value, the relationship was directly correlated. Upon crossing the threshold, the relation became inversely proportional. Therefore, the role of v_s in the evolution of μ_{app} was dependent on P_{avg}. Thus, the P_{avg} was the statistically significant property for the alloys for all lubricants except EML. In the latter case, the trends indicate that μ_{app} is equivalent to the μ_p (friction due to the ploughing action of the asperities). The other components, such as friction due to plastic deformation of the asperities and adhesion, appear to have no influence on μ_{app} using EML. This could be attributed to the high flowrate of the EML, which prevents the build-up of adhesive material on the pins, thereby delivering a consistent μ_{app} under all contact conditions.

Table 8
A comparison of adhesion areas of uncoated and coated pins at 2.30 GPa and 80 m/min and the effect of contact pressure on adhesion for coated pins as seen for Ti-6Al-4V alloy with different lubricants.

Ti-6Al-4V	1.31 GPa and 80 m/min (Coated)	2.30 GPa and 80 m/min (Coated)	2.30 GPa and 80 m/min (Uncoated)	3.27 GPa and 80 m/min (Coated)
Dry	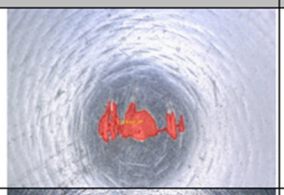	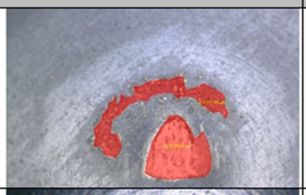	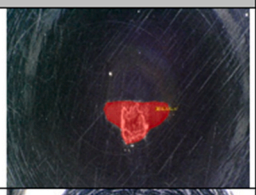	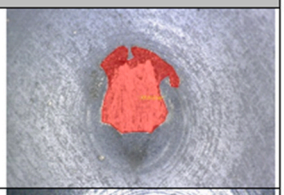
EML	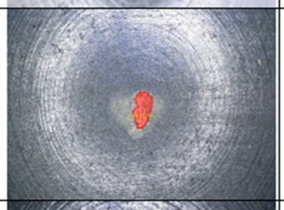	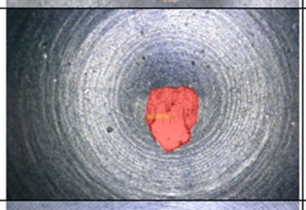		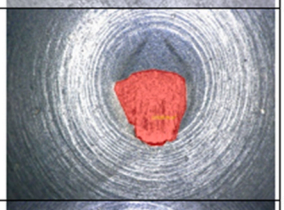
MQLSE1	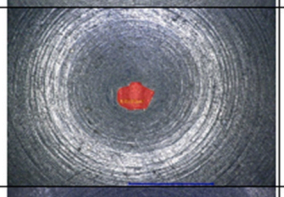	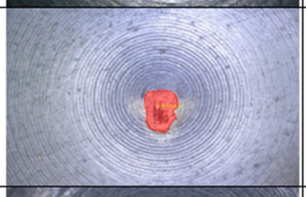	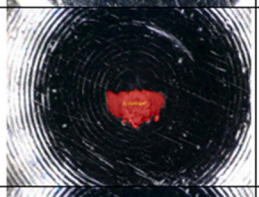	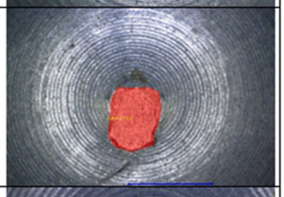
MQLVP	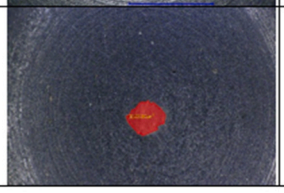	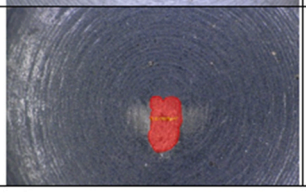	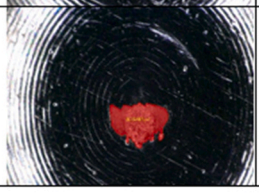	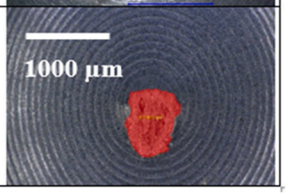

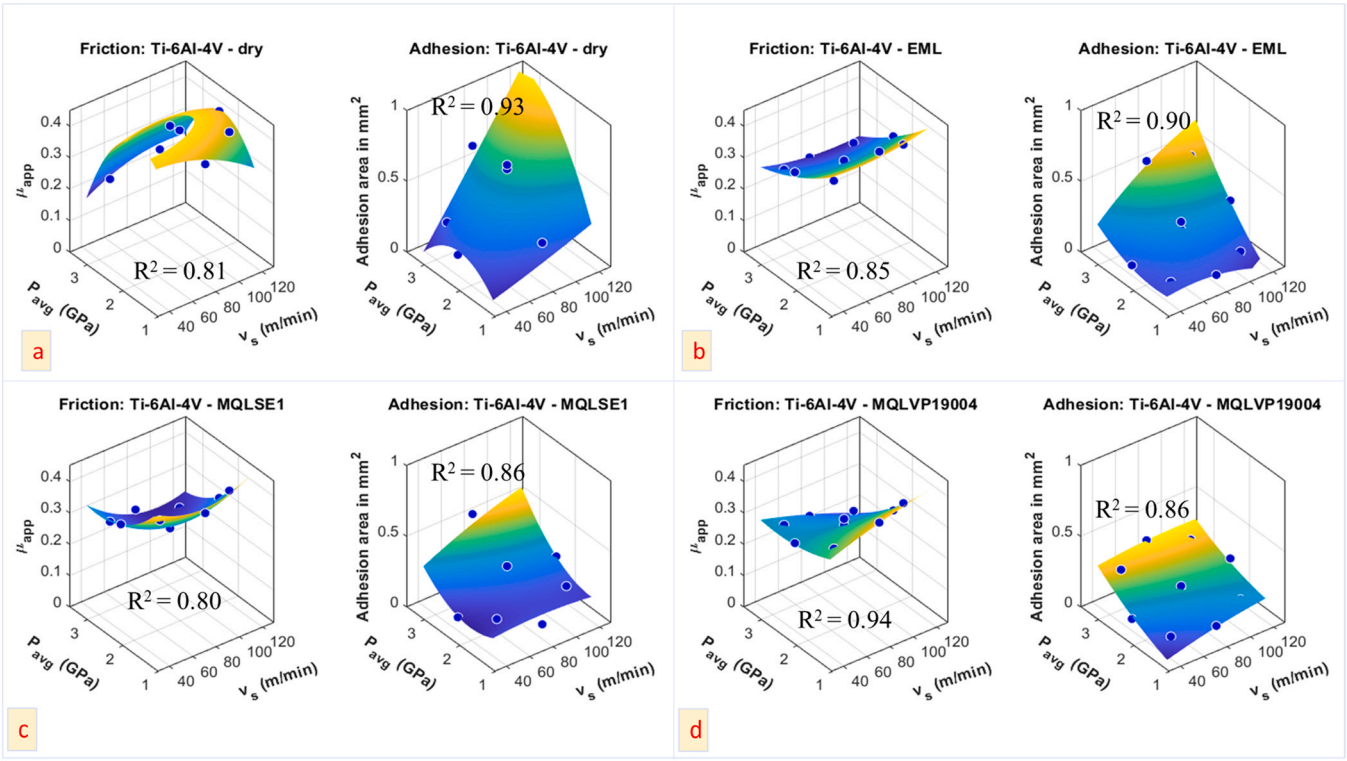

Fig. 8. The friction and adhesion profiles of Ti-6Al-4V with (a) Dry (b) EML (c) MQLSE1 and (d) MQLVP.

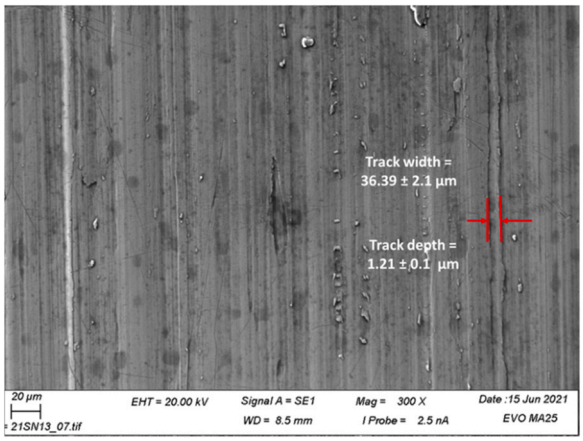

Fig. 9. Track analysis of Ti-6Al-4V in dry condition showing a crack free surface.

Adhesion of Ti-48Al-2Cr-2Nb (near lamellar and duplex)

The adhesion analysis under dry conditions (Figs. 13a and 14a), revealed that when v_s increased from 50 m/min to 110 m/min for 1.61 GPa, only a marginal increase in the adhesion area was recorded (no adhesion at 110 m/min can be considered as an aberration). This means that at a lower P_{avg}, the adhesion area is consistent. This is similar to observations with Ti-6Al-4 V, where no substantial increase in the adhesion area was found by increasing v_s at low P_{avg} values. Conversely, at a higher P_{avg} (3.01 GPa), an increase in v_s from 50 to 110 m/min led to a 3-fold increase in the magnitude of the adhesion area. Importantly, the μ_{app} values at this point remained constant, negating the effect of the increase in the adhesion area.

With EML (Figs. 13b and 14b), the pure errors were low for both alloys, indicating that the experiments were consistent. As observed in dry conditions, the low P_{avg} did not lead to any substantial increase in adhesion or sticking area. At 3.01 GPa, an increase in v_s from 50 to 110 m/min led to an increase in the adhesion area. However, this did not alter the values of μ_{app} substantially. The

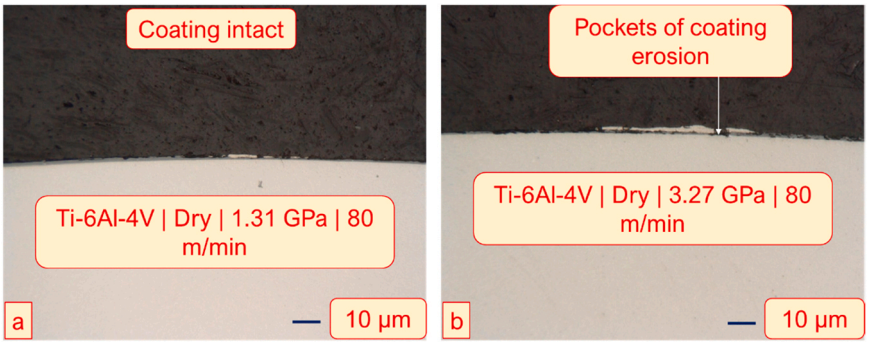

Fig. 10. (a) Coating intact at 1.31 GPa (b) Possible coating erosion at 3.27 GPa, with EML for Ti-6Al-4V alloy.

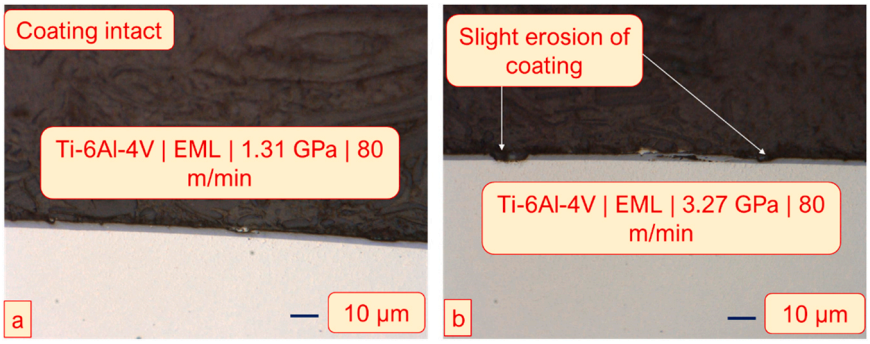

Fig. 11. (a) Coating intact at 1.31 GPa (b) Coating erosion at 3.27 GPa, with EML for Ti-6Al-4V alloy.

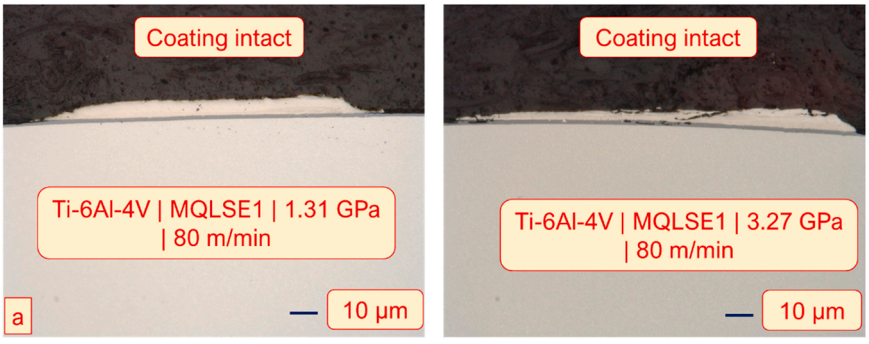

Fig. 12. (a) Coating intact with no damage at 1.31 GPa (b) Coating intact despite few fissures at 3.27 GPa, with MQLSE1 for Ti-6Al-4V alloy.

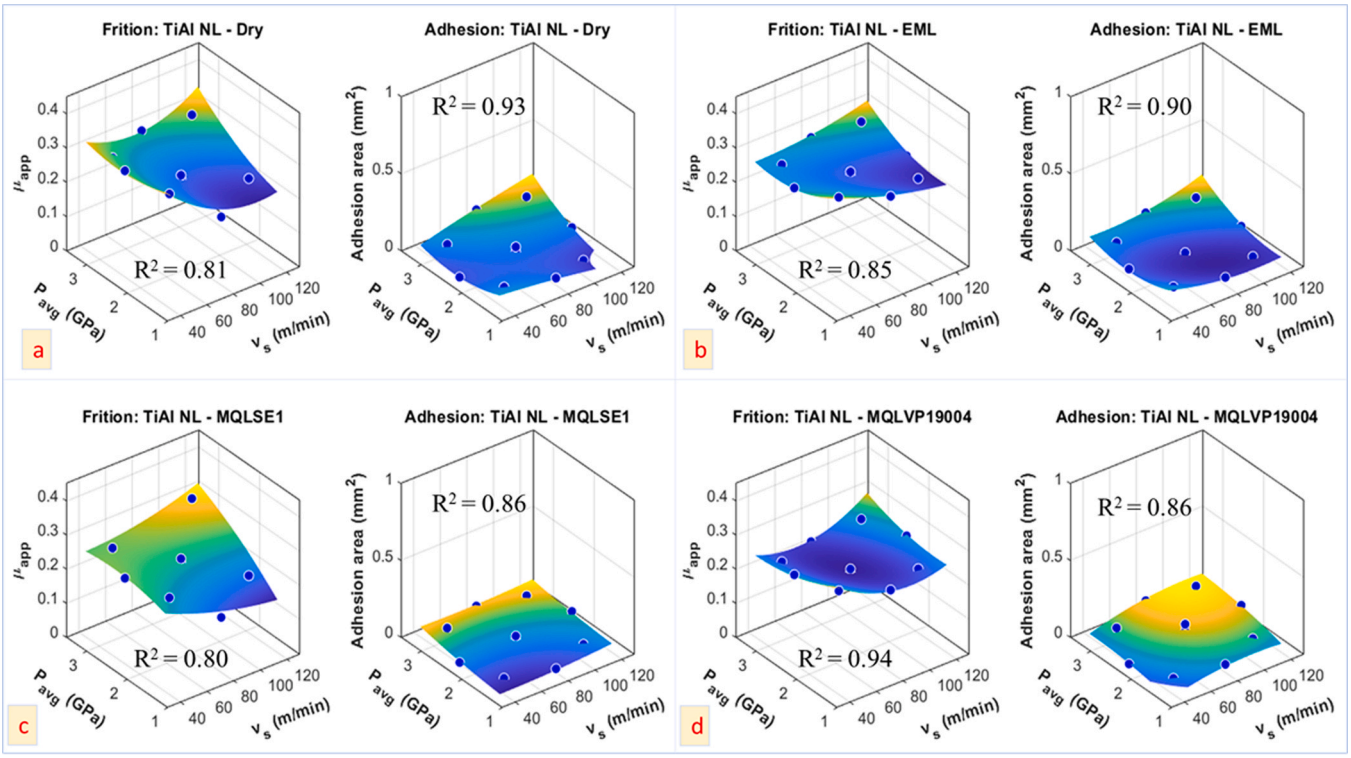

Fig. 13. The friction and adhesion profiles of Ti-48Al-2Cr-2Nb (NL) with (a) dry (b) EML(c) MQLSE1 and (d) MQLVP lubricants.

Table 9
A comparison of adhesion areas of uncoated and coated pins at 2.30 GPa and 80 m/min and the effect of contact pressure on adhesion for coated pins as seen for Ti-48Al-2Cr-2Nb (NL) alloy with different lubricants.

Ti-48Al-2Cr-2Nb (NL)	1.31 GPa and 80 m/min (Coated)	2.30 GPa and 80 m/min (Coated)	2.30 GPa and 80 m/min (Uncoated)	3.27 GPa and 80 m/min (Coated)
Dry	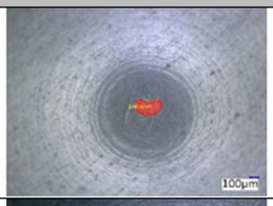	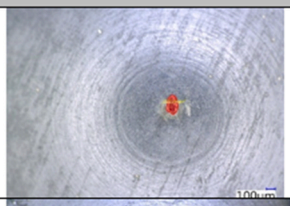		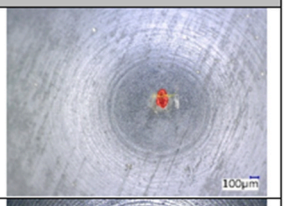
EML	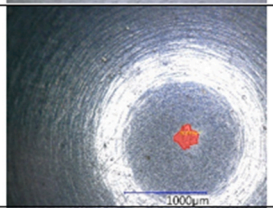	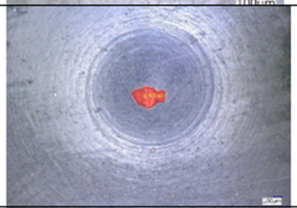		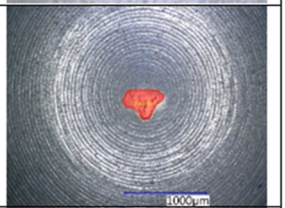
MQLSE1	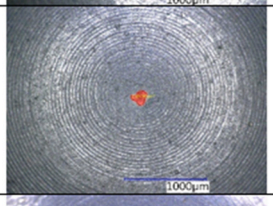	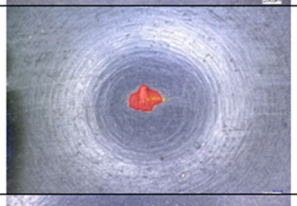	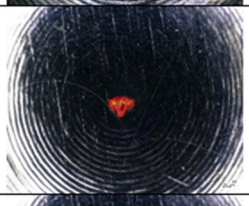	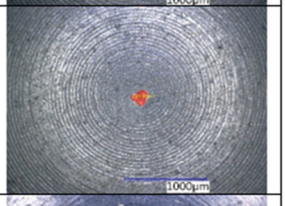
MQLVP	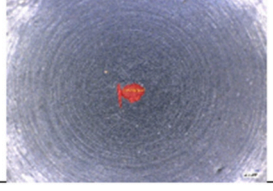	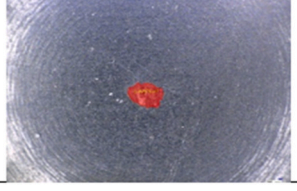	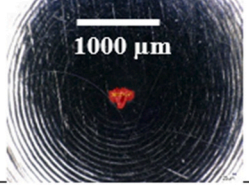	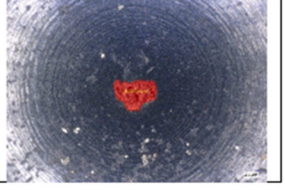

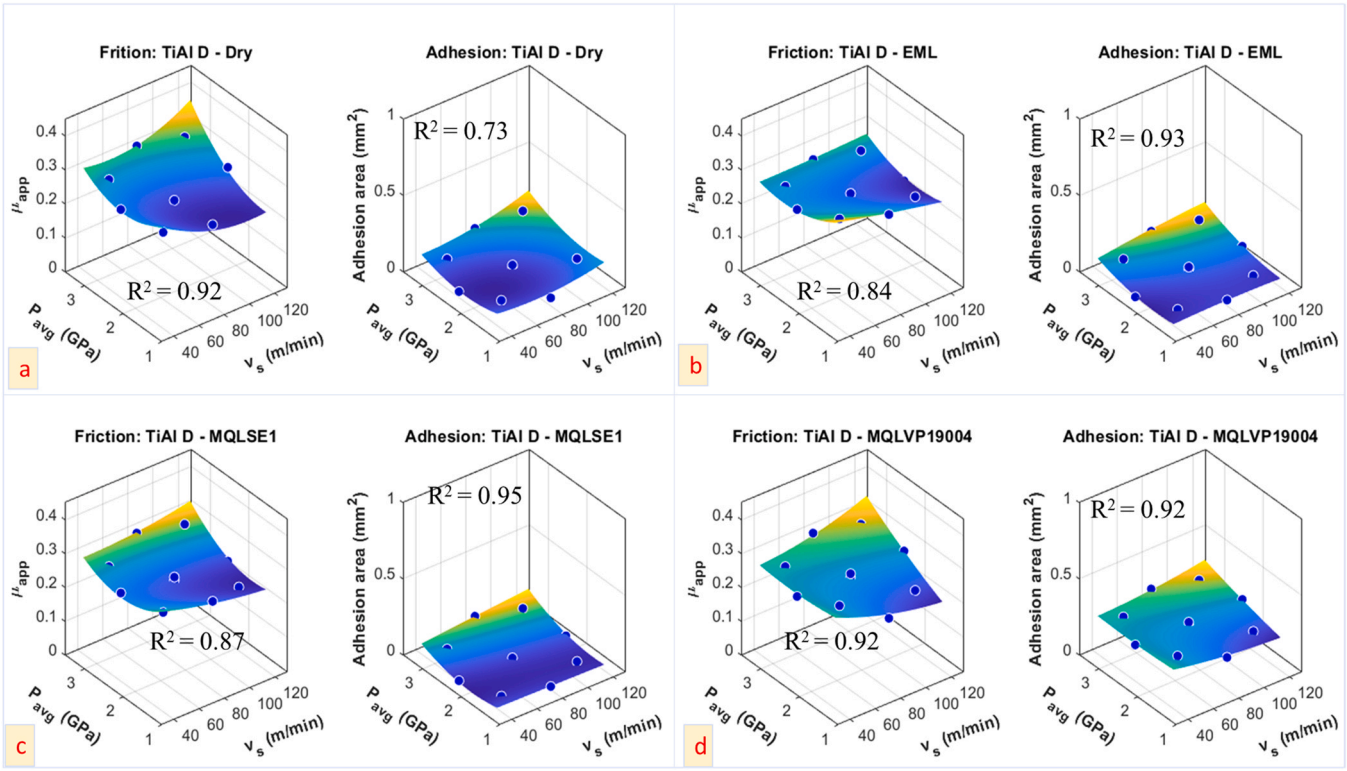

Fig. 14. The friction and adhesion profiles of Ti-48Al-2Cr-2Nb (NL) with (a) dry (b) EML(c) MQLSE1 and (d) MQLVP lubricants.

Table 10
A comparison of adhesion areas of uncoated and coated pins at 2.30 GPa and 80 m/min and the effect of contact pressure on adhesion for coated pins as seen for Ti-48Al-2Cr-2Nb (D) alloy with different lubricants.

Ti-48Al-2Cr-2Nb (D)	1.31 GPa and 80 m/min (Coated)	2.30 GPa and 80 m/min (Coated)	2.30 GPa and 80 m/min (Uncoated)	3.27 GPa and 80 m/min (Coated)
Dry	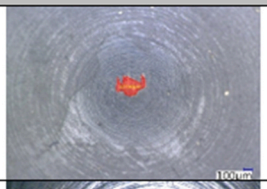	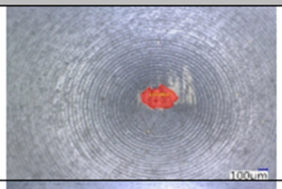	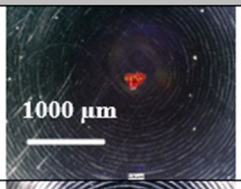	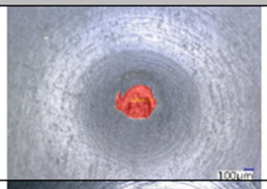
EML	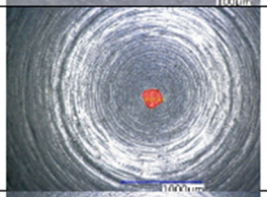	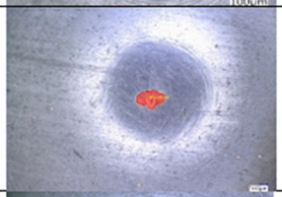	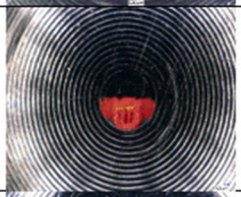	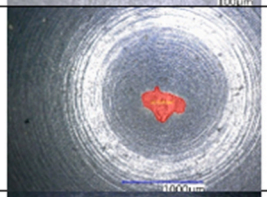
MQLSE1	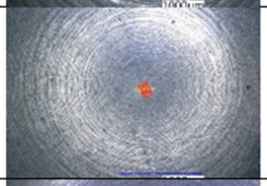	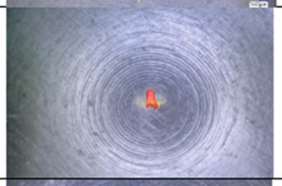	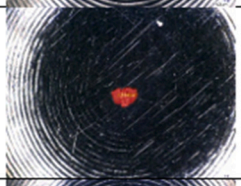	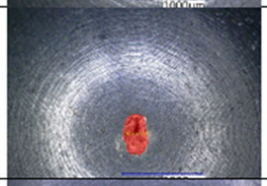
MQLVP	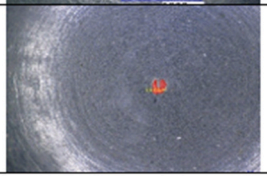	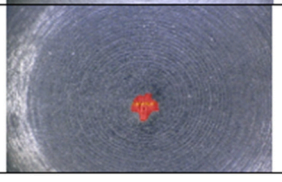	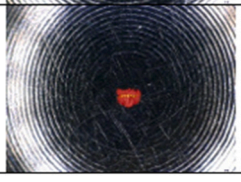	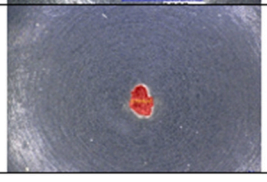

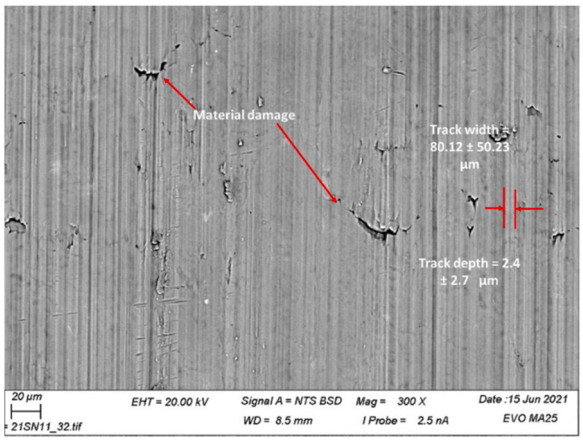

Fig. 15. Track analysis of Ti-48Al-2Cr-2Nb (NL) in dry condition showing a crack-free but damaged surface.

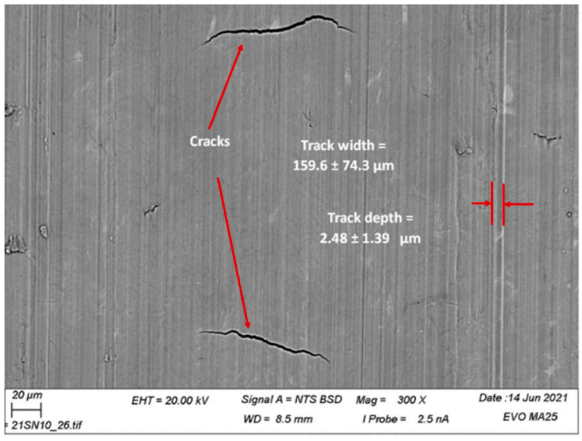

Fig. 16. Track analysis of Ti-48Al-2Cr-2Nb (D) with dry lubrications showing wear track surface w with cracks.

MQLSE1 (Figs. 13c and 14c) and MQLVP (Fig. 13d and Fig. 14d) showed minimum adhesion across the test matrix. Importantly, even at higher P_{avg}, the increase in adhesion values was minimal with increase in v_s. Thus, the friction profile of the Ti-48Al-2Cr-2 Nb (NL and D) alloys were independent of adhesion and lubricants.

For both the alloys, uncoated pins presented higher adhesion area than coated pins. The only exception being the dry conditions and MQLVP for Ti-48Al-2Cr-2 Nb (D) alloy, where similar adhesion profiles were observed. Importantly, though higher adhesion area of uncoated pins was evident, both the pin types presented similar μ_{app} for a given lubricant. Interestingly, both the uncoated and coated pins in dry conditions yielded lower adhesion areas than lubricants. Tables 9 and 10 showcase the comparison of adhesion areas of uncoated and coated pins for both the alloys.

The track analysis of Ti-48Al-2Cr-2 Nb (NL) in dry conditions with uncoated pins, as presented in (Fig. 15), revealed that the material surface was damaged, and defects, such as pullouts, were evident. Interestingly, the rough surface did not translate in increasing the μ_{app}, as both uncoated and coated had similar values.

Another noteworthy observation was the track analysis of Ti-48Al-2Cr-2 Nb (D) alloy. Though, being ductile in comparison to the near lamellar microstructure, the duplex microstructure showed a defect free but cracked surface as shown in Fig. 16. The material surface was smooth with the absence pullouts.

The coating wear analysis showed interesting outcomes for both the alloys. For the Ti-48Al-2Cr-2 Nb (NL) alloy in dry conditions, the coating was found to be intact as seen in Fig. 17a and b. The analysis was conducted on a lower magnification of 20 µm to assess the true extent of the coating wear as material damage and cracks were seen in track analysis. Rest of all the assessments were carried out at a higher magnification of 10 µm. For the Ti-48Al-2Cr-Nb (D) alloy, though the coating was intact at lower P_{avg} of 1.31 GPa (Fig. 17c), some erosion of coating was seen at 3.27 GPa (Fig. 17d).

The EML ensured that coating had the best quality amongst all the lubricants. Both the Ti-48Al-2Cr-2 Nb (NL and D) had their coatings intact at P_{avg} of 1.31 and 3.27 GPa as shown in Fig. 18.

Both the alloys showed good coating quality with MQLSE1. No cavities or any form of degradation were observed even at P_{avg} of 3.27 GPa as seen in Fig. 19.

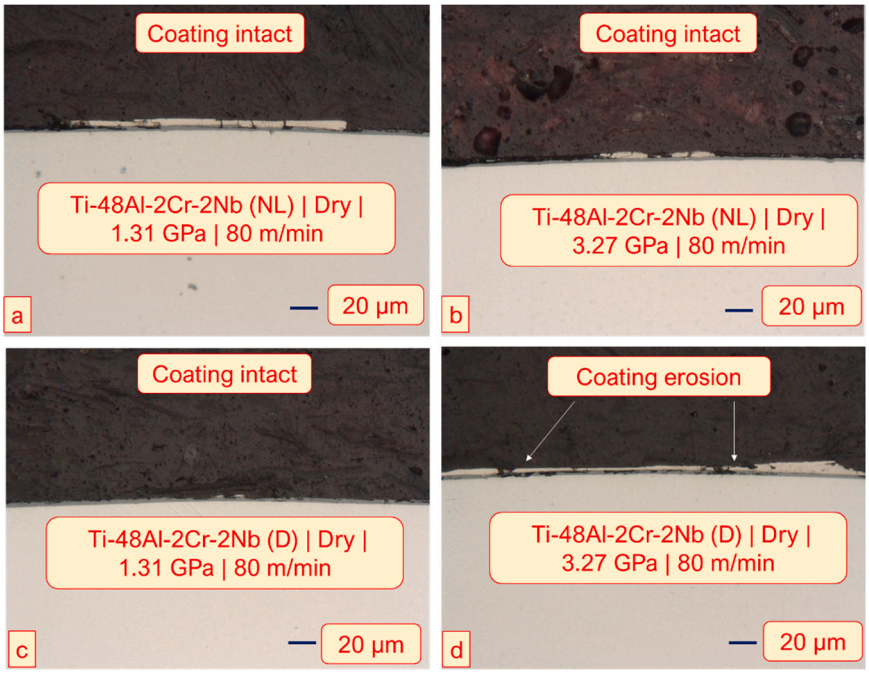

Fig. 17. Coating wear analysis in dry conditions showing a defect free coating of (a–b) Ti-48Al-2Cr-2Nb (NL) and coating erosion of (c-d) Ti-48Al-2Cr-2Nb (D) alloy.

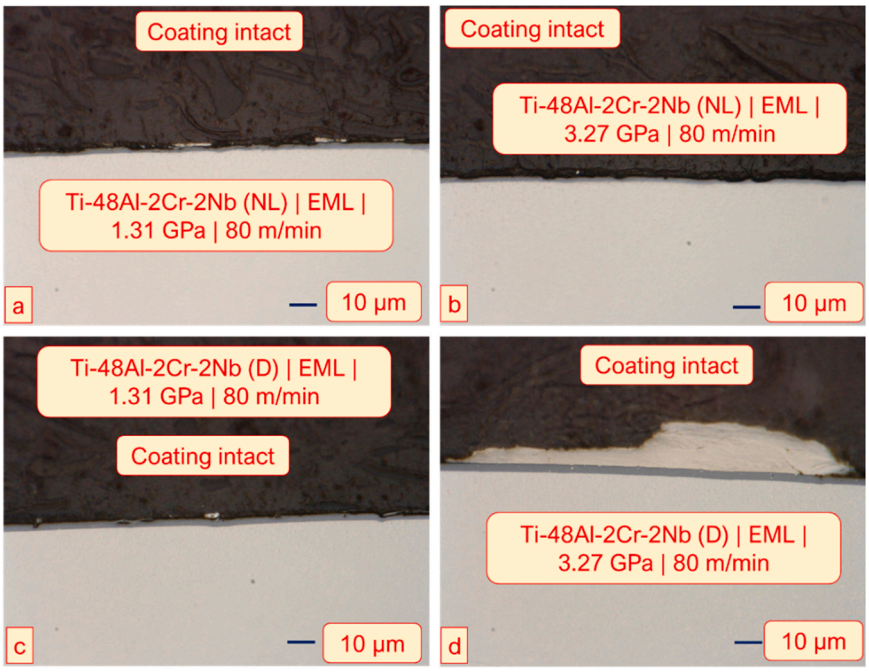

Fig. 18. No damage to the coating observed with EML for (a–b) Ti-48Al-2Cr-2Nb (NL) (c-d) Ti-48Al-2Cr-2Nb (D) alloy.

Thus, both EML and MQLSE1 showed better coating quality and condition as compared to dry condition. Coating wear analysis could not be conducted with MQLVP due to budgetary constraints and unavailability of pins. Thus, no comments could be made on coating quality with MQLVP oil. In addition, the true extent of the coating quality could be assessed only after SEM analysis.

Nevertheless, it is important to analyse why the Ti-48Al-2Cr-2 Nb (NL) alloy shows more or less the same μ_{app} for all contact conditions, particularly for EML and MQLVP lubricants. Suh and Sin [28] in their work have postulated the genesis of friction between sliding surfaces into VI stages, as presented in Fig. 20. In the stage I, the friction is mainly due to the ploughing action of the asperities. As adhesion is absent, no rise in the friction profile is seen at this stage. In the stage II, the friction begins to rise due to the increase in adhesion. This is followed by the stage III, characterised by the rapid increase in the friction due to the high entrapment of the wear particles. A consistency in the adhesion area is reached in the stage IV. Continuing the sliding further, the wear volume decreases causing a fall in the friction in stage V, before reaching a minimum consistent value in stage VI.

The lower μ_{app} values suggest that friction evolution in the Ti-48Al-2Cr-2 Nb (NL) alloy is unable to cross stage I (initial stage) of the friction curve. This is because the adhesion area is more or less constant across the entire test matrix. Thus, stage II and III are absent in current study. Therefore, μ_{app} values represent the kinematic friction coefficient (μ_i)

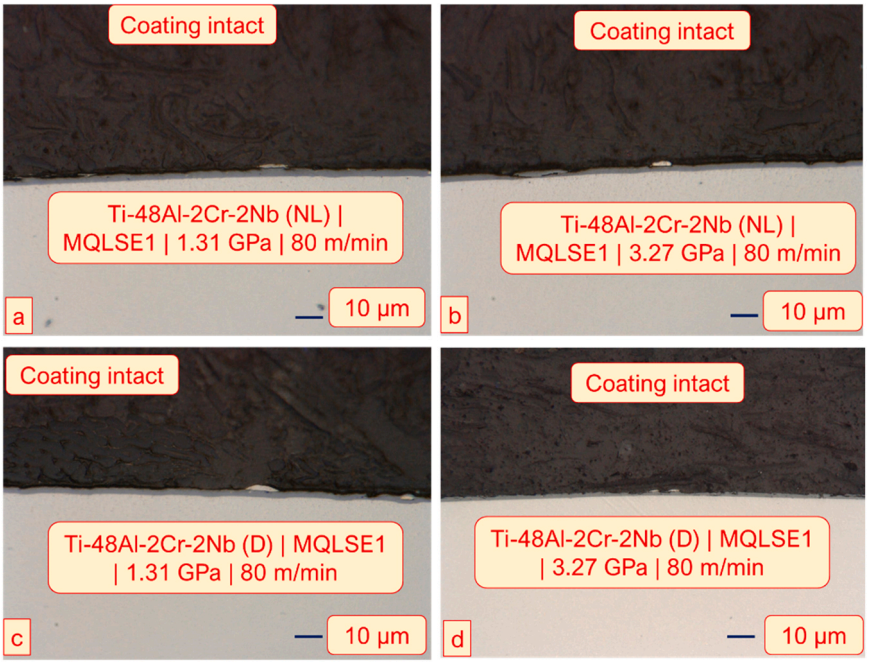

Fig. 19. No damage to coating wear observed with MQLSE1 at (a) 1.31 GPa and (b) 3.27 GPa for Ti-48Al-2Cr-2Nb (NL) alloy.

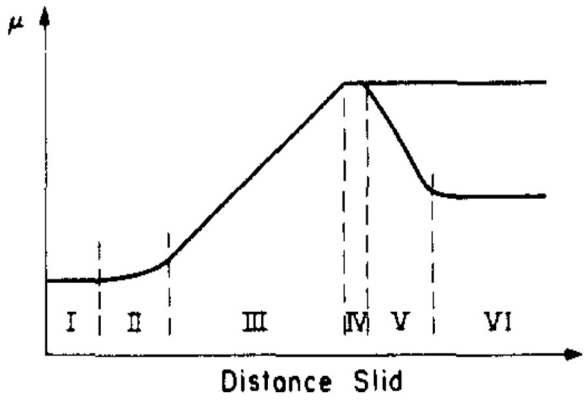

Fig. 20. Different stages in the evolution of friction between sliding bodies [28].

under all contact conditions. The consistency of μ_{app} under all P_{avg} could be due to the high material integrity of the Ti-48Al-2Cr-2 Nb (NL) alloy when combined with EML and MQLVP lubricants, leading to low adhesion of the workpiece to the pins.

The heat partition analysis of the alloys was conducted with coated pins at the threshold conditions of 2.30 GPa + 80 m/min. In dry conditions, where Ti-48Al-2Cr-2 Nb (NL and D) generated 16.27 W and 15.0 W, the Ti-6Al-4 V generated a higher heat of 51.5 W. The thermal conductivity of the Ti-48Al-2Cr-2 Nb alloys (12–13 W/m K) is greater than Ti-6Al-4 V (6.7 W/m K). Surprisingly, 81% of the total heat was transmitted to the pins in the case of Ti-48Al-2Cr-2 Nb alloys, while 70% was transmitted in the case of Ti-6Al-4 V alloys.

As expected, EML reduced the heat transmitted to the pins due to its superior heat extraction properties. Although the quantum of heat generated was similar, a difference of 8% in heat transmission was recorded between the Ti-48Al-2Cr-2 Nb (NL) and Ti-48Al-2Cr-2 Nb (D) alloys. Both microstructures performed similarly with MQLSE1 and MQLVP lubricants. The transmission of heat was higher than EML by 36–46%.

Thus, the heat partition indicated that the EML was best suited to extract the maximum heat during the experiments. The heat generated under dry conditions was higher than that of the other lubricants, and this condition should be avoided because it may lead to thermal shocks to the pins. MQL oils are also effective in heat extraction but are not as effective as EML. This is because of the lubricating effect of MQL oils against the cooling effect of the EML. However, for sliding velocities up to 80 m/min, EML has 20% less heat incident on the pins than MQL oils. Experiments with higher sliding velocities would aid in determining the limitations of MQL oils.

Conclusions

In this study, the tribological properties of friction, adhesion, coating wear, and heat partition were characterised for Ti-6Al-4 V, Ti-48Al-2Cr-2 Nb (Near lamellar), and Ti-48Al-2Cr-2 Nb (Duplex) alloys. A pin-on-cylinder test methodology was adopted with uncoated WC substrate, and WC substrate coated with AlTiSiN pins in dry, flood (EML), MQLSE1, and MQLVP lubricants. The experimental plan was based on a central composite design, with 11 experiments, inclusive of three repetitions at central point of 2.30 GPa + 80 m/min, for each lubricant. The contact conditions were calculated using Hertzian conditions with contact pressures (P_{avg}) between 1.31 and 3.27 GPa and pin sliding velocities (v_s) between 37 and 122 m/min. The results showed:

- The Ti-6Al-4 V alloy generates higher friction, adhesion, and heat than the Ti-48Al-2Cr-2 Nb alloys. All tribological properties of the Ti-48Al-2Cr-2 Nb alloys were found to be independent of the microstructure. P_{avg} was a statistically significant quantity which influenced the tribological properties. On the one hand where an increase in the P_{avg} led to a decrease in the apparent friction coefficient (μ_{app}) for Ti-6Al-4 V alloy, on the other an increase in P_{avg} led to an increase in the friction coefficients of Ti-48Al-2Cr-2 Nb (NL and D) alloys. The role of v_s in affecting the evolution of μ_{app} changed depending on the value of P_{avg}, alloy type, and the lubricant. Additionally, for the Ti-6Al-4 V alloy, an increase in P_{avg} led to an increase in the adhesion area. Concurrently, an increase in P_{avg} led to a decrease in the μ_{app}. Thus, the adhered material lubricated the contacting bodies.
- Negligible adhesion of the workpiece material on to the pins was observed in the case of Ti-48Al-2Cr-2 Nb (NL and D) alloys. The adhered area did not bring any qualitative changes to the friction profile. Thus, the μ_{app} was mainly due to the ploughing action of the asperities. Other components, such as the adhesion and plastic deformation of the asperities, played a very limited role in the evolution of the μ_{app} for both the Ti-48Al-2Cr-2 Nb alloys. Additionally, the change in microstructure of Ti-48Al-2Cr-2 Nb alloy did not affect the tribological properties qualitatively nor quantitatively.
- Notably, the AlTiSiN coating played either a detrimental (Ti-6Al-4 V) or negligible role (Ti-48Al-2Cr-2 Nb NL and D) in decreasing the μ_{app}. This work utilised tribological characterisation to prove that machining Ti-48Al-2Cr-2 Nb alloys is a heat-intensive process. Machining under dry conditions can deliver thermal shocks, leading to a shortened tool life. Therefore, it is prudent to avoid these conditions during commercial manufacturing of titanium aluminides. Flood lubricants (EML) and MQL provide similar tribological outcomes and are suitable for machining Ti-48Al-2Cr-2 Nb alloys.

Funding

No specific funding was received for the publication of this article.

CRediT authorship contribution statement

Abhishek V. Hukkerikar: Conceptualization, Methodology, Investigation, Formal analysis, Data curation, Software, Visualization, Validation, Writing – original draft, Writing – review & editing. **Pedro-J. Arrazola**: Conceptualization, Methodology, Formal analysis, Project administration, Supervision, Writing – review & editing, Resources. **Patxi Aristimuño**: Conceptualization, Methodology, Formal analysis, Project administration, Supervision, Writing – review & editing. **Susanne Norgren**: Investigation, Project administration, Writing – review & editing, Validation, Resources. **Antoine Morandeau**: Conceptualization, Methodology, Investigation, Software, Review. **Damien Joly**: Investigation, Validation, Review.

Conflict of interest

The authors state that there is no conflict of interest whatsoever, to the best of their knowledge.

Acknowledgements

The authors would like to thank the organisations of Access e.V. (Germany), Blaser Swisslube (Switzerland), and AB Sandvik Coromant (Sweden). The authors would also like to extend a special thanks to Todor Stoyanov (Access), Tobias Mathys (Blaser Swisslube), Pär Lindberg (Sandvik Coromant), Sinuhé Hernández (Sandvik Coromant), Adnan Mahmood (Sandvik Coromant), and David Blurtsyan (Sandvik Coromant) for their contributions and facilitation during the course of this work.

Appendix A

The uncertainties observed during friction characterisation.

Alloy	Absolute uncertainty in friction characterization			
	Dry	EML	MQLSE1	MQLVP
Coated				
NL	0.005	0.05	0.05	0.05
D	0.01	0.05	0.05	0.05
Ti64	0.01	0.05	0.01	0.01
Uncoated				
NL	0.005	0	0.05	0
D	0.005	0	0.05	0
Ti64	0	0.05	0.05	0.01

Appendix B

Absolute uncertainty from adhesion measurements of the Ti-48Al-2Cr-2Nb (Near lamellar and Duplex) and Ti-6Al-4V alloys with dry, EML, MQLSE1 and MQLVP lubricants.

Alloy	Absolute uncertainty in adhesion measurement (mm^2)			
	Dry	EML	MQLSE1	MQLVP
Coated				
NL	0.005	0.05	0.01	0.025
D	0.02	0.02	0.005	0.02
Ti64	0.22	0.035	0.08	0.01
Uncoated				
NL	0.006	0.005	0.005	0.01
D	0.01	0.03	0.005	0
Ti64	0.03	0.02	0.03	0.005

Appendix C

Regression analysis and contour plots.

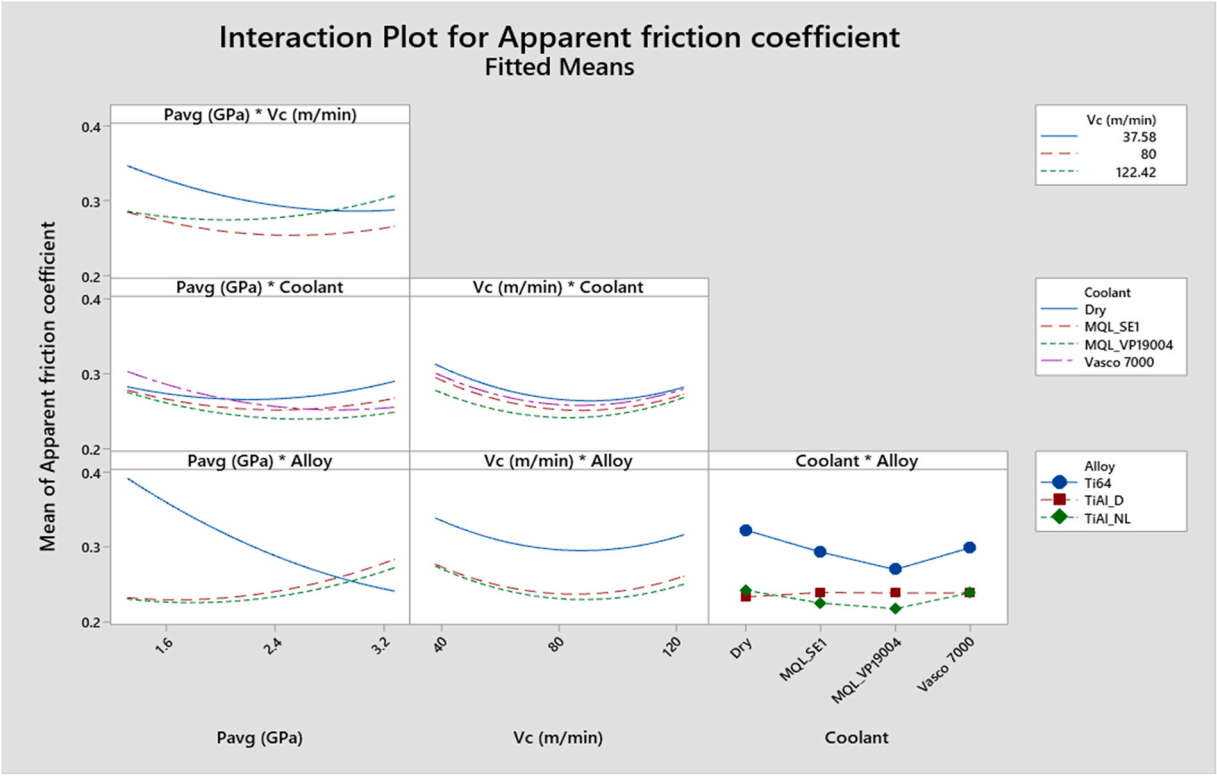

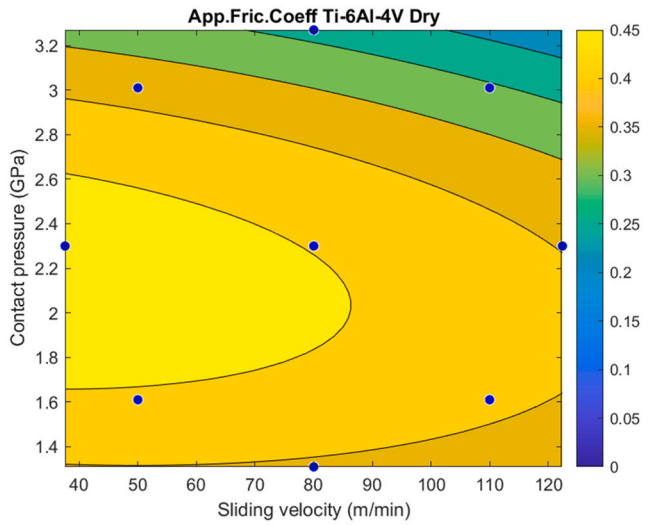
App.Fric.Coeff Ti-6Al-4V Dry
Contact pressure (GPa)
Sliding velocity (m/min)

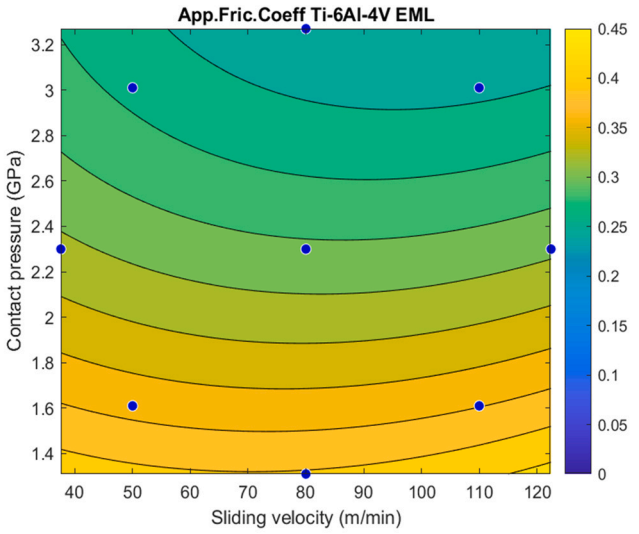
App.Fric.Coeff Ti-6Al-4V EML
Contact pressure (GPa)
Sliding velocity (m/min)

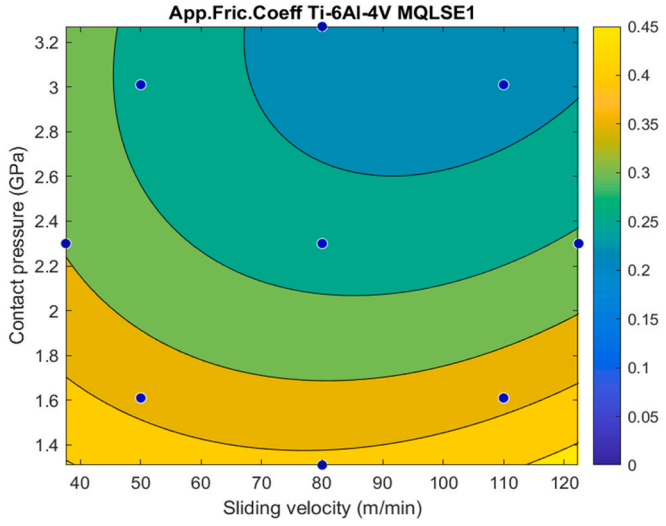
App.Fric.Coeff Ti-6Al-4V MQLSE1
Contact pressure (GPa)
Sliding velocity (m/min)

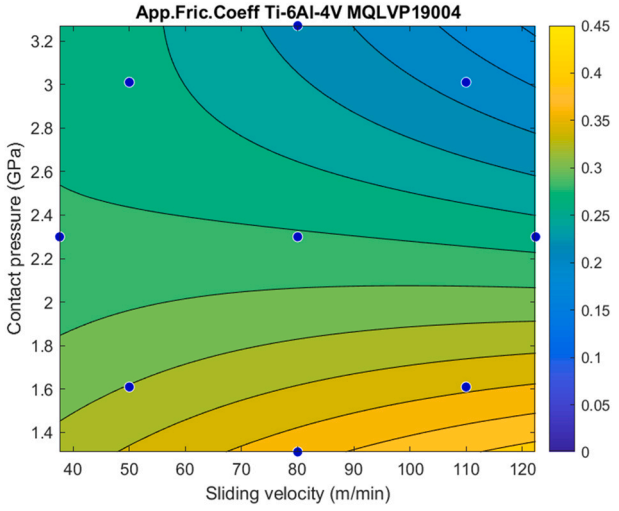
App.Fric.Coeff Ti-6Al-4V MQLVP19004
Contact pressure (GPa)
Sliding velocity (m/min)

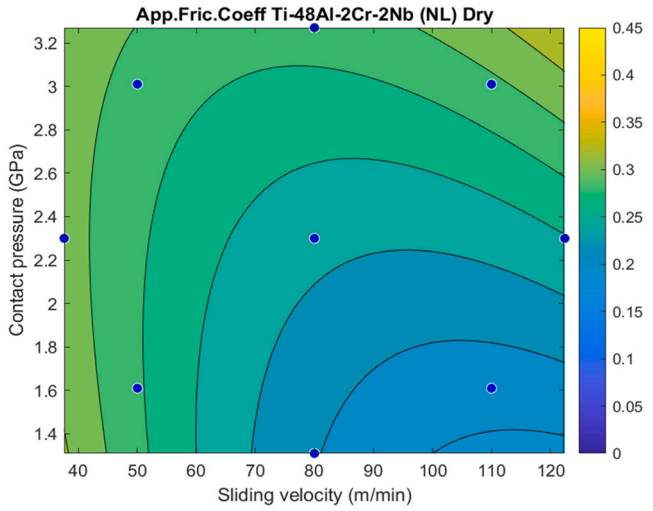
App.Fric.Coeff Ti-48Al-2Cr-2Nb (NL) Dry
Contact pressure (GPa)
Sliding velocity (m/min)

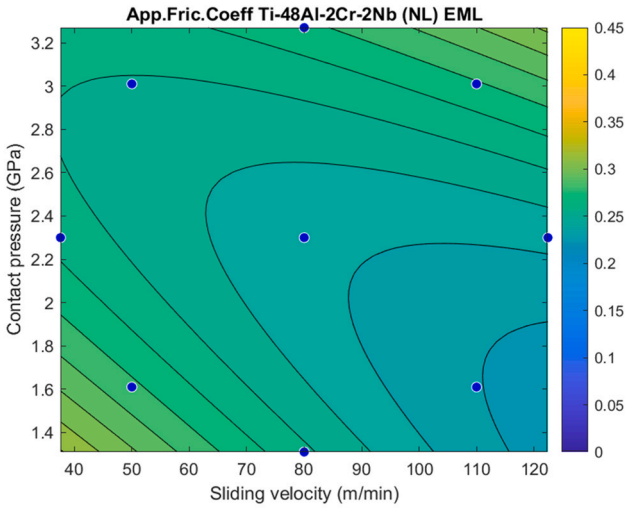
App.Fric.Coeff Ti-48Al-2Cr-2Nb (NL) EML
Contact pressure (GPa)
Sliding velocity (m/min)

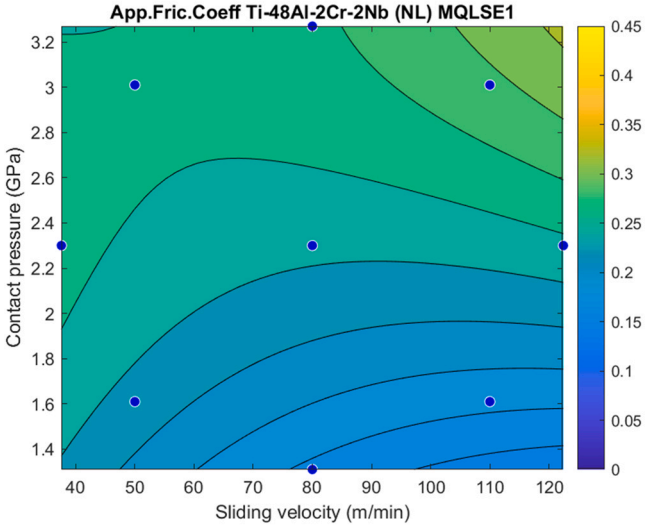
App.Fric.Coeff Ti-48Al-2Cr-2Nb (NL) MQLSE1
Contact pressure (GPa)
Sliding velocity (m/min)

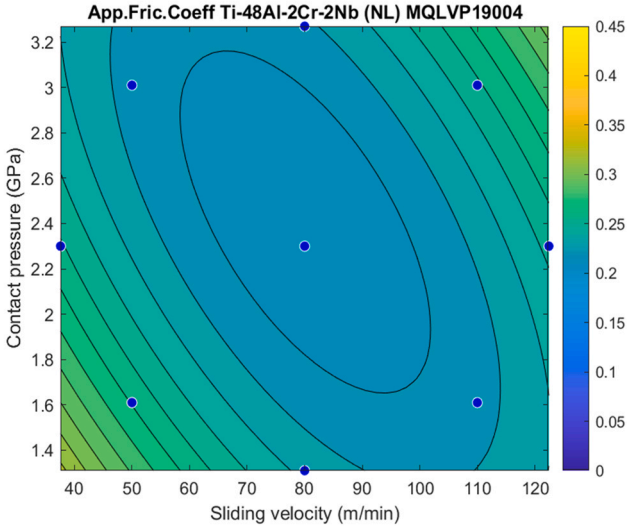
App.Fric.Coeff Ti-48Al-2Cr-2Nb (NL) MQLVP19004
Contact pressure (GPa)
Sliding velocity (m/min)

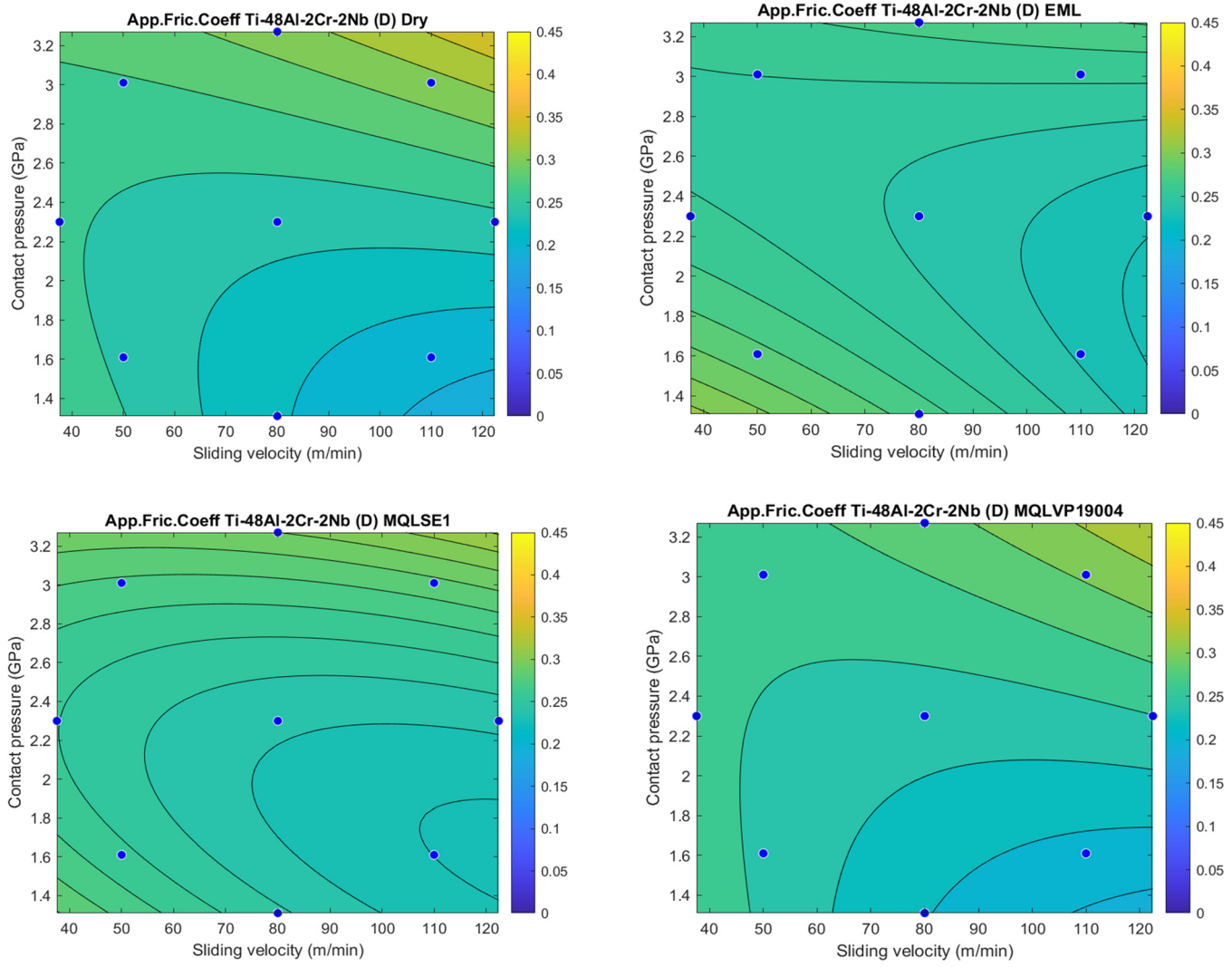

References

[1] Appel, F., Paul, J.D.H., Oehring, M., 2011. Gamma titanium aluminide alloys: science and technology. Gamma Titanium Aluminide Alloys: Science and Technology. ⟨https://doi.org/10.1002/9783527636204⟩.

[2] Arrazola, P.J., Ugarte, D., Dominguez, X., 2008, A new approach for the friction identification during machining through the use of finite element modeling. International Journal of Machine Tools & Manufacture, 48:173–183. https://doi.org/10.1016/j.ijmachtools.2007.08.022.

[3] Aspinwall, D.K., Mantle, A.L., Chan, W.K., Hood, R., Soo, S.L., 2013, Cutting temperatures when ball nose end milling γ-TiAl intermetallic alloys. CIRP Annals, 62/1: 75–78. https://doi.org/10.1016/j.cirp.2013.03.007.

[4] Bewlay, B.P., Nag, S., Suzuki, A., Weimer, M.J., 2016, TiAl alloys in commercial aircraft engines. Materials at High Temperatures, 33/4–5: 549–559. https://doi.org/10.1080/09603409.2016.1183068.

[5] Bhibhansu, N., 2019. Thermo-Mechanical Processing of Third Generation γ – Titanium Aluminides (Issue July). Indian Institute of Science.

[6] Bonnet, C., Valiorgue, F., Rech, J., Claudin, C., Hamdi, H., Bergheau, J.M., Gilles, P., 2008, Identification of a friction model—Application to the context of dry cutting of an AISI 316L austenitic stainless steel with a TiN coated carbide tool. International Journal of Machine Tools and Manufacture, 48/11: 1211–1223. https://doi.org/10.1016/j.ijmachtools.2008.03.011.

[7] Brookes, S., 2009. Thermo-mechanical fatigue behaviour of the near-γ- titanium aluminide alloy TNB-V5 under uniaxial and multiaxial loading. BAM Bundesanstalt für Materialforschung und -prüfung. ⟨https://doi.org/ISBN978-3-9812910-5-6⟩.

[8] Budynas, R., Nisbett, J.K., 2015. Shigley's mechanical engineering design. Mechanical Engineering. ⟨https://doi.org/10.1007/s13398-014-0173-7.2⟩.

[9] Cavazzuti, M., 2013, Optimization Methods: From Theory to Design. Springer-Verlag Berlin Heidelberg.

[10] Claudin, C., Rech, J., Grzesik, W., Zalisz, S., 2008, Characterization of the frictional properties of various coatings at the tool/chip/workpiece interfaces in dry machining of AISI 4140 steel. International Journal of Material Forming, 1/S1: 511–514. https://doi.org/10.1007/s12289-008-0172-3.

[11] Claudin, C., Mondelin, A., Rech, J., Fromentin, G., 2010, Effects of a straight oil on friction at the tool–workmaterial interface in machining. International Journal of Machine Tools and Manufacture, 50/8: 681–688. https://doi.org/10.1016/j.ijmachtools.2010.04.013.

[12] Dimiduk, D., 1999, Gamma titanium aluminide alloys—an assessment within the competition of aerospace structural materials. Materials Science and Engineering: A, 263/2: 281–288. https://doi.org/10.1016/S0921-5093(98)01158-7.

[13] Gupta, R.K., Pant, B., Sinha, P.P., 2014, Theory and practice of γ + α2 Ti aluminide: A review. Transactions of the Indian Institute of Metals, 67/2: 143–165. https://doi.org/10.1007/s12666-013-0334-y.

[14] International Civil Aviation Organization Envisioning a Zero Climate Impact International Aviation Pathwaytowards 2050: How Governments and the Aviation Industry Can Step-up amidst the Climate Emergency for A Sustainable Aviation Future (No. A40-WP/561; EX/238).

[15] Klocke, F., Lung, D., Arft, M., Priarone, P.C., Settineri, L., 2013, On high-speed turning of a third-generation gamma titanium aluminide. International Journal of Advanced Manufacturing Technology. https://doi.org/10.1007/s00170-012-4157-5.

[16] Kolahdouz, S., Hadi, M., Arezoo, B., Zamani, S., 2015, Investigation of surface integrity in high speed milling of gamma titanium aluminide under dry and minimum quantity lubricant conditions. Procedia CIRP, 26:367–372. https://doi.org/10.1016/j.procir.2014.08.016.

[17] Kothari, K., 2010. Manufacturing Techniques for Titanium Aluminide Based Alloys and Metal Matrix Composites (Doctoral thesis). University of Maryland, College Park, MD, 20742. ⟨https://apps.dtic.mil/dtic/tr/fulltext/u2/a631137.pdf⟩.

[18] Li, C.X., Xia, J., Dong, H., 2006, Sliding wear of TiAl intermetallics against steel and ceramics of Al2O3, Si3N4 and WC/Co. Wear. https://doi.org/10.1016/j.wear.2006.01.044.
[19] Lutjering, G., Williams, J.C., 2007. Titanium, second ed. Engineering Materials and Processes.
[20] Melkote, S.N., Grzesik, W., Outeiro, J., Rech, J., Schulze, V., Attia, H., Arrazola, P.-J., M'Saoubi, R., Saldana, C., 2017, Advances in material and friction data for modelling of metal machining. CIRP Annals, 66/2: 731–754. https://doi.org/10.1016/j.cirp.2017.05.002.
[21] Milton, S., Duchosal, A., Chalon, F., Leroy, R., Morandeau, A., 2019, Thermal study during milling of Ti6Al4V produced by Electron Beam Melting (EBM) process. Journal of Manufacturing Processes, 38/August 2018: 256–265. https://doi.org/10.1016/j.jmapro.2018.12.027.
[22] Milton, S., 2018. Study on the Machinability and Surface Integrity of Ti6Al4V Produced by Selective Laser Melting (SLM) and Electron Beam Melting (EBM) Processes.
[23] Ortiz-de-Zarate, G., Madariaga, A., Arrazola, P.J., Childs, T.H.C., 2021, A novel methodology to characterize tool-chip contact in metal cutting using partially restricted contact length tools. CIRP Annals, 70/1: 61–64. https://doi.org/10.1016/j.cirp.2021.03.002.
[24] Priarone, P.C., Robiglio, M., Settineri, L., Tebaldo, V., 2014, Milling and Turning of Titanium Aluminides by Using Minimum Quantity Lubrication. Procedia CIRP, 24:62–67. https://doi.org/10.1016/j.procir.2014.07.147.
[25] Rastkar, A.R., Bell, T., 2005, Characterization and tribological performance of oxide layers on a gamma based titanium aluminide. Wear. https://doi.org/10.1016/j.wear.2004.11.014.
[26] Settineri, L., Priarone, P.C., Arft, M., Lung, D., Stoyanov, T., 2014, An evaluative approach to correlate machinability, microstructures, and material properties of gamma titanium aluminides. CIRP Annals, 63/1: 57–60. https://doi.org/10.1016/j.cirp.2014.03.068.
[27] Shih, D.S., Huang, S.C., Scarr, G.K., Jang, H., Chestnut, J.C., 1991. Microstructural Dependence Of Mechanical Properties of Ti-48Al-2Cr-2Nb.
[28] Suh, N.P., Sin, H.-C., 1981, The genesis of friction. Wear, 69/1: 91–114. https://doi.org/10.1016/0043-1648(81)90315-X.
[29] Takeyama, M., Kobayashi, S., 2005, Physical metallurgy for wrought gamma titanium aluminides: Microstructure control through phase transformations. Intermetallics. https://doi.org/10.1016/j.intermet.2004.12.014.
[30] Zemzemi, F., Bensalem, W., Rech, J., Dogui, A., Kapsa, P., 2008, New tribometer designed for the characterisation of the friction properties at the tool/chip/workpiece interfaces in machining. Tribotest, 14/1: 11–25. https://doi.org/10.1002/tt.50.